



$^{40}\text{Ar}/^{39}\text{Ar}$ dating and cosmic-ray exposure time of desert meteorites: Dhofar 300 and Dhofar 007 eucrites and anomalous achondrite NWA 011

Ekaterina V. KOROCHANTSEVA^{1,2}, Mario TRIELOFF^{1*}, Alexei I. BUIKIN^{1,2},
Jens HOPP¹, and Hans-Peter MEYER¹

¹Mineralogisches Institut, Ruprecht-Karls-Universität Heidelberg, Im Neuenheimer Feld 236, D-69120 Heidelberg, Germany

²Vernadsky Institute of Geochemistry, Kosygin Street 19, 119991 Moscow, Russia

*Corresponding author. E-mail: trieloff@min.uni-heidelberg.de

(Received 21 April 2005; revision accepted 13 May 2005)

Abstract—We performed high-resolution ^{40}Ar - ^{39}Ar dating of mineral separates and whole-rock samples from the desert meteorites Dhofar 300, Dhofar 007, and Northwest Africa (NWA) 011. The chronological information of all samples is dominated by plagioclase of varying grain size. The last total reset age of the eucrites Dhofar 300 and Dhofar 007 is 3.9 ± 0.1 Ga, coeval with the intense cratering period on the Moon. Some large plagioclase grains of Dhofar 007 possibly inherited Ar from a 4.5 Ga event characteristic for other cumulate eucrites. Due to disturbances of the age spectrum of NWA 011, only an estimate of 3.2–3.9 Ga can be given for its last total reset age. Secondary events causing partial ^{40}Ar loss ≤ 3.4 Ga ago are indicated by all age spectra. Furthermore, Ar extractions from distinct low temperature phases define apparent isochrons for all samples. These isochron ages are chronologically irrelevant and most probably caused by desert alterations, in which radiogenic ^{40}Ar and K from the meteorite and occasionally K induced by weathering are mixed, accompanied by incorporation of atmospheric Ar. Additional uptake of atmospheric Ar by the alteration phase(s) was observed during mineral separation (i.e., crushing and cleaning in ultrasonic baths). Consistent cosmic-ray exposure ages were obtained from plagioclase and pyroxene exposure age spectra of Dhofar 300 (25 ± 1 Ma) and Dhofar 007 (13 ± 1 Ma) using the mineral's specific target element chemistry and corresponding ^{38}Ar production rates.

INTRODUCTION

Impact cratering is the most important geological process in the evolution of solar system bodies after early accretion, heating, differentiation, and cooling. The influence of shock metamorphism on the textural, mineralogical, chemical, and isotopic properties of terrestrial and extraterrestrial rocks have been well studied in recent decades (e.g., Melosh 1989; Stöffler et al. 1991; French 1998). A prominent example demonstrating the importance of surface evolution by impact cratering, is the so-called “lunar cataclysm” forming the large ring basins on the Moon at about 3.8–4.0 Ga ago (Tera et al. 1974; Hartmann 1975; Baldwin 1974; Turner 1977; Jessberger 1982; Ryder 1990; Stöffler and Ryder 2001). Certain meteorite parent bodies were likely affected by this early impact activity as well, e.g., the howardite-eucrite-diogenite (HED) parent body (Bogard 1995; Kunz et al. 1995) or Mars (Turner et al. 1997), contrary to ordinary chondrite parent bodies. Bogard (1995) pointed out that the intense bombardment by late, large projectiles

may be recorded more strongly by larger parent bodies such as the Moon or the asteroid Vesta (which is most probably the HED parent body) (e.g., Ruzicka et al. 1997 and references therein). Only large bodies can survive large impacts and are severely affected by accompanying heating effects that reset radiometric systems because larger craters produce a higher proportion of impact melt (Grieve and Cintala 1992).

Due to its relatively low closure temperature, the K-Ar system is sensitive and thus suitable to record cratering events. The ^{40}Ar - ^{39}Ar dating technique has been widely used to investigate the thermal history and impact chronology of the HED parent body (Podosek and Huneke 1973; Kaneoka et al. 1979, 1995; Takeda et al. 1994; Bogard 1995; Kunz et al. 1995; Bogard and Garrison 2003). Bogard (1995) considers that most eucrites and howardites show impact reset of ^{40}Ar - ^{39}Ar ages between 4.1–3.4 Ga ago. The ages of several cumulate and unbrecciated eucrites cluster at ~ 4.48 Ga, probably reflecting an early large impact on the HED parent body followed by a rapid cooling (Bogard and Garrison 2003). Obviously, this eucrite type suffered less

intense impact reset during the subsequent collisional history. On the contrary, brecciated and noncumulate eucrites were more influenced by late impact metamorphism, inducing brecciation and variable reset of the K-Ar system. These effects were studied by Kunz et al. (1995), who analyzed ten different lithic clasts from five brecciated eucrites. They demonstrated that different clasts recorded impact events differently or had a significant individual pre-history. Based on the age information of individual constituents, Kunz et al. (1995) suggested a more intense bombardment of the HED parent body ~4.4–3.9 Ga ago and a time of less intense impact-induced metamorphism ~3.9–2.8 Ga ago.

Besides the HED parent body, the parent body of Northwest Africa (NWA) 011 also causes great interest concerning its thermal history. NWA 011 was originally classified as a noncumulate eucrite with an anomalous Fe/Mn (69 atomic) ratio (Afanasiev et al. 2000). Based on the chemistry and oxygen isotopic composition, Yamaguchi et al. (2002) concluded that NWA 011 is a new type of basaltic meteorite, genetically different from eucrites. Palme (2002) suggested that NWA 011 could be of Mercurian origin. However, Yamaguchi et al. (2002) and Nyquist et al. (2003) assumed that NWA 011 came from the asteroid belt. Its parent body composition was suggested to be close to carbonaceous chondrites (Boesenberg 2003; Bogdanovski and Lugmair 2004). Due to the relatively large size of the NWA 011 parent body (Bogdanovski and Lugmair 2004), NWA 011 was expected to possibly record late large impacts events. The meteorite's texture indicates recrystallization, possibly as a result of thermal metamorphism. Since this rock has some common features with eucrites (Afanasiev et al. 2000), it is interesting to compare their collisional histories.

Here we report a ^{40}Ar - ^{39}Ar case study of two eucrites (Dhofar 300 and Dhofar 007) recently discovered in the desert of Oman (Grossman and Zipfel 2001; Afanasiev et al. 2000) and the unique achondrite NWA 011. Since eucrite age spectra often have complex fine structure, we performed high-resolution ^{40}Ar - ^{39}Ar stepwise heating analyses on whole rock samples and handpicked mineral separates of the Dhofar eucrites, including plagioclase, pyroxene, and vein glass. In this way, we aimed at determining the response of different minerals to the various possible effects affecting the K-Ar system of eucrites: partial ^{40}Ar loss, ^{39}Ar recoil redistribution (Huneke and Smith 1976; Turner and Cadogan 1974; Kunz et al. 1995), weathering, and contamination by terrestrial atmospheric Ar.

EXPERIMENTAL TECHNIQUES

Polished thin sections of Dhofar 300 (~90 mm²), Dhofar 007 (~2 cm²; ~6 mm²), and NWA 011 (~3 cm²) were studied using traditional methods of optical microscopy in transmitted and reflected light. Mineral compositions were determined with the CAMEBAX Microbeam at the

Vernadsky Institute, Moscow, Russia, and the CAMECA SX51 electron microprobe at the Mineralogical Institute of the University of Heidelberg, Heidelberg, Germany (Table 1). The analyses were performed at 15 keV accelerating voltage, 20 nA beam current, and 20 sec counting time.

Dhofar 300 and Dhofar 007 samples weighing 1.55 g and 2.03 g, respectively, were crushed and powdered in an agate mortar to measure major element contents at the Vernadsky Institute. Calcium was measured by X-ray fluorescence (XRF) in 500 mg portions of the powders. Calcium was also determined in 100 mg duplicates of the powders by inductively coupled plasma-atomic emission spectrometry (ICP-AES). Bulk Ca concentrations are given in Table 2 for comparison with ^{40}Ar - ^{39}Ar data; other chemical data will be given elsewhere.

Mineral separates (plagioclase, pyroxene, and Dhofar 007 vein glass) were prepared by mechanical separation using a binocular. ^{40}Ar - ^{39}Ar analysis followed standard procedures given by Jessberger et al. (1980) and Trierloff et al. (1994, 1998). Samples were wrapped in high-purity (99.999%) aluminum foil and irradiated behind cadmium shielding for 27 days in an evacuated quartz ampoule at the GKSS-reactor in Geesthacht, Germany. The J-value was 1.52×10^{-2} , as determined by NL25 hornblende flux monitors (Schaeffer and Schaeffer 1977). Correction factors for interfering isotopes determined by CaF_2 monitors were $(^{36}\text{Ar}/^{37}\text{Ar})_{\text{Ca}} = (4.6 \pm 0.1) \times 10^{-4}$, $(^{38}\text{Ar}/^{37}\text{Ar})_{\text{Ca}} = (8.8 \pm 0.2) \times 10^{-5}$, $(^{39}\text{Ar}/^{37}\text{Ar})_{\text{Ca}} = (9.6 \pm 0.1) \times 10^{-4}$. $(^{38}\text{Ar}/^{39}\text{Ar})_{\text{K}} = (1.88 \pm 0.13) \times 10^{-2}$ was determined via the NL25 monitors, after subtraction of Cl-induced ^{38}Ar . $(^{40}\text{Ar}/^{37}\text{Ar})_{\text{Ca}} = (3 \pm 3) \times 10^{-3}$ was determined by Turner (1971) and $(^{40}\text{Ar}/^{39}\text{Ar})_{\text{K}} = (1.23 \pm 0.24) \times 10^{-2}$ by Brereton (1970). The samples were stepwise heated to temperatures from 300 °C to 1650 °C (up to 34 temperature steps) using an induction-heated furnace with ^{40}Ar blank values of $(1.7 - 4) \times 10^{-10}$ ccSTP at 1000 °C and $(1.8 - 15) \times 10^{-10}$ ccSTP at 1400 °C (10 min heating duration). Apparent ages were calculated using the Steiger and Jäger (1977) conventions. Given uncertainties are 1σ .

SAMPLE DESCRIPTIONS

Dhofar 300 was found in the desert of Oman in 2001 and was classified as a eucrite (Grossman and Zipfel 2001). Petrography and mineral chemistry of this rock are based on this work and include some of our data. The meteorite has a light gray color and is weathered and rusted. Dhofar 300 is a monomict breccia consisting of millimeter-size (0.5–5 mm) lithic clasts (~70 vol%) set within a fragmental matrix (Fig. 1a). Lithic clasts are characterized by textural variations. Ophitic to subophitic clasts have mineral grain sizes up to ~300 μm and coarse-grained granular clasts up to ~800 μm. Clasts are composed of plagioclase, very finely exsolved pyroxene, and minor low-Ca pyroxene. The matrix mainly consists of single mineral fragments of plagioclase

Table 1. Chemical composition of plagioclase and pyroxene from Dhofar 300, Dhofar 007, and NWA 011 by electron microprobe (average and variations, wt%).

	SiO ₂	TiO ₂	Al ₂ O ₃	Cr ₂ O ₃	FeO ^a	MnO	MgO	CaO	Na ₂ O	K ₂ O	Total	En or Ab	Wo or An	Fs or Or
Dhofar 300														
Plagioclase ^b	46.2		34.3		0.68 ^c		0.14 ^c	17.1	1.39	0.10	99.9	12.7	86.7	0.6
n = 37 ^d	44.2–48.9		32.2–36.9		0.11–3.40		b.d. ^e –1.02	15.2–18.9	0.64–2.35	b.d.–0.43		5.8–20.7	77.9–94.0	0–2.5
Low-Ca pyroxene ^b	49.3	0.23	0.23	0.28	36.5	1.26	11.6	1.16			100.6	34.5	2.5	63.1
n = 23	48.5–49.9	0.16–0.28	0.15–0.31	0.04–0.97	34.5–38.1	0.93–2.96	11.0–12.4	0.75–2.01				33.5–36.4	1.6–4.4	61.2–64.5
Clasts														
High-Ca pyroxene	49.3	0.35	0.34	0.82	28.2	1.14	10.4	9.50			100.0	30.8	20.3	49.0
n = 15	48.7–50.8	0.20–0.59	0.15–0.52	0.29–1.48	22.0–32.3	0.73–1.73	9.9–11.1	5.2–16.3				29.2–32.87	11.2–34.0	36.8–57.1
Matrix														
Augite	50.2	0.37	0.40	0.49	18.4	0.51	10.1	19.3			99.7	29.2	40.1	30.7
n = 11	48.8–51.3	0.15–0.96	0.27–0.55	0.06–1.17	16.8–22.9	0.38–0.75	9.3–10.8	15.6–20.9				27.2–30.9	32.6–43.7	27.9–38.7
Dhofar 007 (coarse-grained clasts)														
Plagioclase	45.4		34.3		0.22			18.6	0.91	0.04	99.4	8.1	91.6	0.3
n = 15	44.8–46.0		33.8–34.7		0.07–0.55			18.3–18.8	0.77–1.13	0.02–0.07		6.9–9.9	89.7–92.9	0.1–0.4
Pyroxene ^f	51.3	0.40	0.79	0.53	25.2	0.81	16.6	4.37	0.03		100.0	48.4	9.1	42.4
n = 18	50.4–51.8	0.29–0.51	0.60–0.90	0.41–0.61	24.5–25.7	0.71–0.93	16.3–17.1	3.86–4.79	b.d.–0.05			47.7–49.7	8.1–10.0	41.3–43.9
NWA 011														
Plagioclase	45.3		35.9		0.43			17.2	1.48	0.08	100.3	13.4	86.1	0.5
n = 93	42.0–48.7		31.6–39.0		0.15–2.81			15.1–18.9	0.81–2.50	0.03–0.13		7.2–22.4	76.9–92.6	0.2–0.8
Pyroxene ^f	50.0	0.49	0.85	0.29	30.9	0.47	9.51	7.23	0.06		99.8	29.5	16.1	54.4
n = 37	48.4–51.4	0.26–0.73	0.68–1.01	0.11–0.44	28.3–34.1	0.32–0.60	9.06–10.00	4.80–8.17	0.01–0.09			28.0–31.1	12.3–18.2	51.8–58.3

^aAll Fe as FeO.

^b Includes analyses of large grains and matrix grains.

^cOccasionally high Mg and Fe concentrations in plagioclase are caused by pyroxene exsolution dots.

^dn: number of analyses.

^eb.d.: below detection.

^fDefocused beam analyses in order to compare with K and Ca contents by Ar-Ar analyses. Includes high-Ca exsolutions plotted in Fig. 2.

Table 2. Summary of results from ^{40}Ar - ^{39}Ar dating of desert achondrites Dhofar 300, Dhofar 007, and NWA 011. Argon concentrations are given in units of 10^{-8}ccmSTP/g .

	Dhofar 300			Dhofar 007				NWA 011
	WR	Pl	Px	WR	Pl	Px	Glass	WR
LT-age ^a (Ga)	0–1	3.0 ± 0.2	1.8 ± 0.5	3.4 ± 0.2	3.4 ± 0.2			0.80 ± 0.06
HT-age ^a (Ga)	3.9 ± 0.1	3.9 ± 0.1	3.9 ± 0.1	3.9 ± 0.2	4.5 ± 0.2			3.2–3.9
$^{36}\text{Ar}_{\text{trapped}}$	0.46	1.95	1.51	0.40	1.75	0.66	4.50	0.336
$^{36}\text{Ar}_{\text{spall}}$	2.23	3.78	1.52	1.01	1.87	0.58	0.88	2.847
$^{38}\text{Ar}_{\text{trapped}}$	0.085	0.364	0.282	0.075	0.327	0.115	0.840	0.063
$^{38}\text{Ar}_{\text{spall}}$	3.424	5.821	2.345	1.559	2.877	0.892	1.367	4.380
$^{38}\text{Ar}_{\text{Chlorine}}$	0.002	–	–	0.015	0.080	0.011	0.063	–
K (ppm)	328 ± 9	767 ± 21	55 ± 2	104 ± 3	297 ± 8	14 ± 3	65 ± 3	217 ± 6
K_{EMPA} (ppm)		830			373			~249 ^b
Ca (%)	6.81 ± 0.19	12.52 ± 0.35	4.16 ± 0.13 (3.28 in Px)	6.62 ± 0.16	11.9 ± 0.3	2.7 ± 0.4	4.18 ± 0.17	7.75 ± 0.22
Ca_{EMPA} (%)	7.3 ^c	12.2	5.8 ^d	7.5 ^c	13.3	3.1 ^d		7.69 ^b
Plagioclase content ^e (%)	43		7	35		<4.7 ^f		
Pyroxene content (%)	57		93	65		>95		
Sample weight (mg)	114	17	22.9	81.4	10.7	20.8	5.1	96.6

^aApparent ages at low temperature extractions (LT) and high temperature extractions (HT), respectively.

^bEstimated from $\text{K}_2\text{O} = 0.03$ (wt%) given by Korochantseva et al. (2003).

^cThe average whole rock values are average of XRF and ICP-AES data.

^dCa concentration of pyroxene was calculated using EMPA average pyroxene analyses and a ratio (high/low Ca Px) = 5 for Dhofar 300, but is difficult to compare with the sample used for ^{40}Ar - ^{39}Ar dating because of unknown proportions of clasts and matrix and exact modal composition of high- and low-Ca pyroxene within them. For Dhofar 007, defocused beam analyses are shown (see also Table 1), the agreement is good, but bulk Ca content from ^{40}Ar - ^{39}Ar data can also be influenced by Ca-poor accessories.

^eFrom ^{39}Ar derived K content of pyroxene or whole rock compared to plagioclase.

^fThe maximum abundance of plagioclase impurities is given, assuming all K is derived from plagioclase. However, the release pattern does not support this assumption.

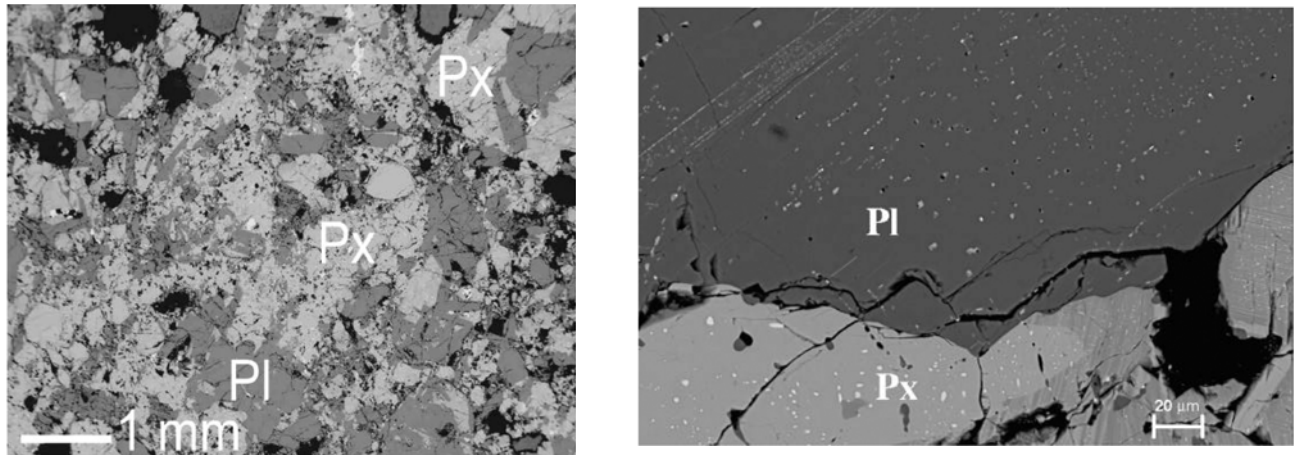


Fig. 1. a) The texture of Dhofar 300, a BSE image. Plagioclase (dark gray phase) is of variable size. b) Dhofar 300 plagioclase is clouded by pyroxene in plagioclase (light stripes and dots). Dhofar 300 pyroxene is clouded by sub-micrometer inclusions of opaques. A BSE image.

grains, Cr-bearing augite, and low-Ca pyroxene. Minor minerals are silica, ilmenite, troilite, and Ca phosphate. Shock features include mechanical twinning in pyroxenes and rare planar deformation features in plagioclase.

The chemical compositions of pyroxene and plagioclase in Dhofar 300 clasts and matrix are shown in Table 1. The compositions of plagioclase and low-Ca pyroxene in the lithic clasts and the matrix are similar. Contrary to the clasts, the matrix does not contain pyroxenes of intermediate, falling between low-Ca pyroxene and augite compositions like some other eucrites, e.g., Stannern and Camel Donga (Metzler et al. 1995). All pyroxene compositions plot close to a single orthopyroxene-augite tie line, similar to that for pyroxenes of the Haraiya eucrite (Fig. 2a). The maximum chemical variations within single feldspar grains are 4 mol% of An. The wide range of Dhofar 300 plagioclase compositions indicates that the metamorphic event causing pyroxene equilibration did not effectively equilibrate plagioclase compositions. The clouded appearance of pyroxene and plagioclase grains is distinctly visible. Plagioclase grains are clouded by needles and micrometer-size dots of pyroxene, while pyroxenes are clouded by fine exsolution dots of opaques (Fig. 1b). Harlow and Klimentidis (1980) regard clouding in pyroxene and plagioclase to be the result of exsolution of minor components that became incompatible and crystallized on microfractures and other nucleation sites during post-brecciation metamorphism.

Dhofar 007 was discovered in 1999 in the Dhofar region of Oman (Afanasiev et al. 2000). Examining the cut surfaces ($\sim 125 \text{ cm}^2$) of Dhofar 007, we observe that it is a brecciated meteorite dominantly composed of large (centimeter-size) lithic clasts cemented by a tiny amount of fine-grained fragmental matrix. Millimeter-size clasts are rare. The clasts are characterized by variations of grain size: from relatively fine-grained to very coarse-grained. The abundance of FeNi metal varies from one clast to another. Some clasts are very rich in metal (see also Yamaguchi et al. 2003). Veins of

impact melt discordantly cross the meteorite, causing local darkening. The impact-melt veins are up to $\sim 7 \text{ mm}$ thick. Petrographic investigation of a thin section revealed that the veins are very fine-grained; microporphyric pyroxene crystals ($10\text{--}40 \mu\text{m}$) occur within an ophitic pyroxene-plagioclase matrix (Fig. 3a). Single pyroxene and feldspar fragments are commonly present in the veins.

Based on mineralogical and petrographic observations and correlations of Mg# and Sm content, Afanasiev et al. (2000) showed that Dhofar 007 is a cumulate eucrite, while Yamaguchi et al. (2003) discussed pros and cons of an origin from the mesosiderite or eucrite parent body. Although initially classified as monomict, Yamaguchi et al. (2003) found xenolithic components in Dhofar 007 (an impact melt clast, a Mg-rich orthopyroxene fragment, and recrystallized plagioclase), thereby demonstrating the polymict nature of this rock. They also demonstrated that Dhofar 007 has a high abundance of FeNi metal grains and a very high bulk Ni and Co contents compared with other eucrites.

We investigated two coarse-grained clasts with high abundances of FeNi metal, since this type of clast dominates the rock. The coarse-grained clasts have gabbroic texture and consist of subhedral grains ($0.2\text{--}0.8 \text{ mm}$) of pyroxene and plagioclase occurring in about equal proportions (Fig. 3b). Accessories include silica, metal, troilite, chromite, Ca phosphate, and weathering products. FeNi metal occurs as $50\text{--}200 \mu\text{m}$ grains, usually associated with troilite and mainly located at grain boundaries of plagioclase and pyroxene grains. Pyroxene is mainly low-Ca-pyroxene ($\text{En}_{49.9-52.8}\text{Fs}_{43.1-45.8}\text{Wo}_{2.9-4.7}$) and contains thin augite lamellae ($\text{En}_{42.2-44.7}\text{Fs}_{24.4-27.0}\text{Wo}_{28.3-32.0}$). The lamellae are closely spaced and very fine, but sometimes they are up to $\sim 10 \mu\text{m}$ wide. The bulk composition of pyroxene obtained by defocused beam analyses is presented in Table 1 and is characterized by Mg# = 53–55, and Fe/Mn = 27–35 (atomic). Pyroxene compositions are shown in Fig. 2a. Yamaguchi et al. (2003) also reported an orthopyroxene grain ($\text{Wo}_{1.3}\text{En}_{83.0}$) in a

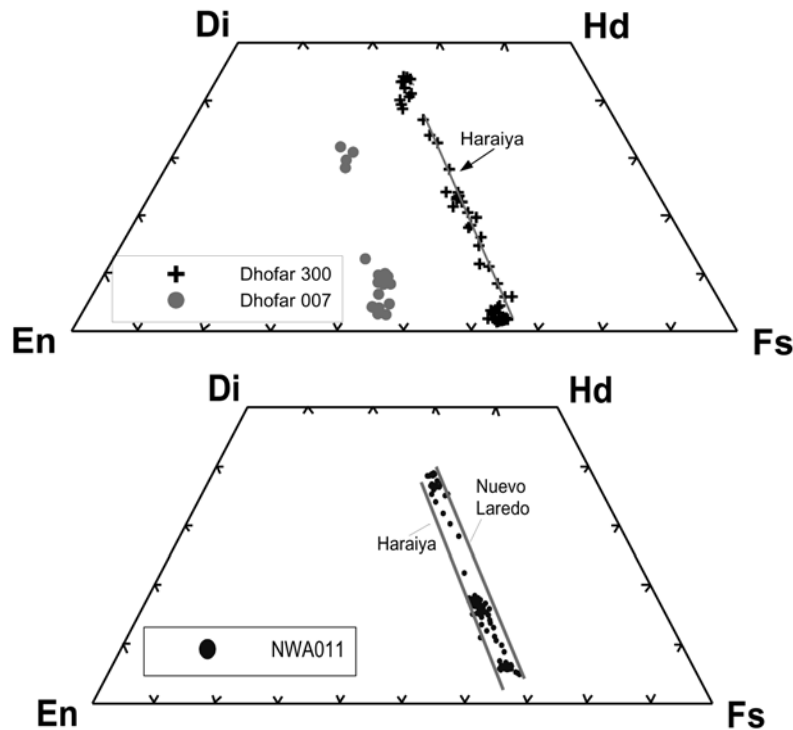


Fig. 2. Pyroxene compositions of Dhofar 300 and Dhofar 007 (a) and NWA 011 (b). Data for Haraiya and Nuevo Laredo (gray lines) were taken from Warren et al. (1987, 1990).

coarse-grained clast. Plagioclase is anorthite, and the K_2O content is low (Table 1). The silicates of Dhofar 007 are pure and transparent when compared to those of Dhofar 300. Chromite is characterized by $Cr/(Cr + Al) = 0.78$ and $Fe\# = 0.95$. FeNi metal is kamacite (Ni 5.0 wt%) and taenite (Ni 43.1 wt%).

NWA 011 was found as a single stone (40 g) in the Sahara desert in 1999. It consists of coarse-grained anhedral pigeonite and rare plagioclase grains (0.2–0.8 mm in size) cemented by a fine-grained (50–100 μm in size) granular plagioclase-pigeonite matrix. The matrix mineral grains display 120° triple junctions indicating intensive recrystallization. Most of pigeonite grains contain exsolution lamellae of augite, usually a few microns wide, but sometimes reaching $\sim 10 \mu m$. Accessories are ulvöspinel, ilmenite, silica, Fe-rich olivine, Ca phosphates, tiny grains of troilite, and FeNi metal-sulfide intergrowths. Ilmenite is closely associated with ulvöspinel forming oxide assemblages. Fe-rich olivine is present also in the assemblages. Rare baddeleyite inclusions (up to 15 μm in size) occur in some ilmenite grains. Ca phosphates and silica minerals are distributed unevenly in this meteorite and are generally associated with plagioclase. Mineral modes (in vol%) are: 58.5 pigeonite, 39.6 plagioclase, 0.71 opaques, 0.67 silica, and 0.54 phosphates. The rock is relatively fresh, but Fe hydroxides are present and replace troilite. Cracks and mineral fractures are filled with the same kind of substances. No features indicating shock metamorphism were found.

The compositions of pigeonite ($En_{28.66-31.3}Fs_{62.08-66.41}Wo_{4.93-7.19}$; $Mg\# = 0.30-0.34$) and augite lamellae ($En_{25.05-27.65}Fs_{34.83-40.55}Wo_{32.03-38.86}$; $Mg\# = 0.39-0.44$) plot close to a single orthopyroxene-augite tie line, similar to pyroxenes of Nuevo Laredo and Haraiya (Fig. 2b). The bulk composition (defocused beam analyses) of pyroxene grains in NWA 011 is presented in Table 1 and is characterized by $Mg\# \sim 0.36$. The Fe/Mn atomic ratios of pigeonite (~ 68) and augite (~ 70) are significantly higher than those of typical eucrites. Plagioclase of NWA 011 is bytownite and is low in K_2O (Table 1). The composition of large plagioclase grains does not differ from that of fine-grained plagioclase. Plagioclase compositions are within the range for noncumulate eucrites. Plagioclase grains are pure and transparent. Olivine is Fe-rich and varies from $Fa_{79.5}$ to $Fa_{84.5}$ (Promprated et al. 2003; Yamaguchi et al. 2002). Ulvöspinel is characterized by $Fe/(Fe + Mg) = 0.98$, contents of TiO_2 , Cr_2O_3 , and Al_2O_3 (in wt%) are 25.8, 11.4, and 4.2, respectively. In ilmenite, FeO, TiO_2 , MnO, and Cr_2O_3 contents (wt%) are 47.6, 51.0, 0.37, and 0.95, respectively. Phosphates are whitlockite and Cl apatite, the latter contains 3.5 wt% of Cl.

RESULTS AND DISCUSSION

Table 2 summarizes the analytical results of our study obtained by $^{40}Ar-^{39}Ar$ step-heating dating. Detailed tables with concentrations of Ar isotopes and apparent ages for each temperature extraction are given in the Appendix tables.

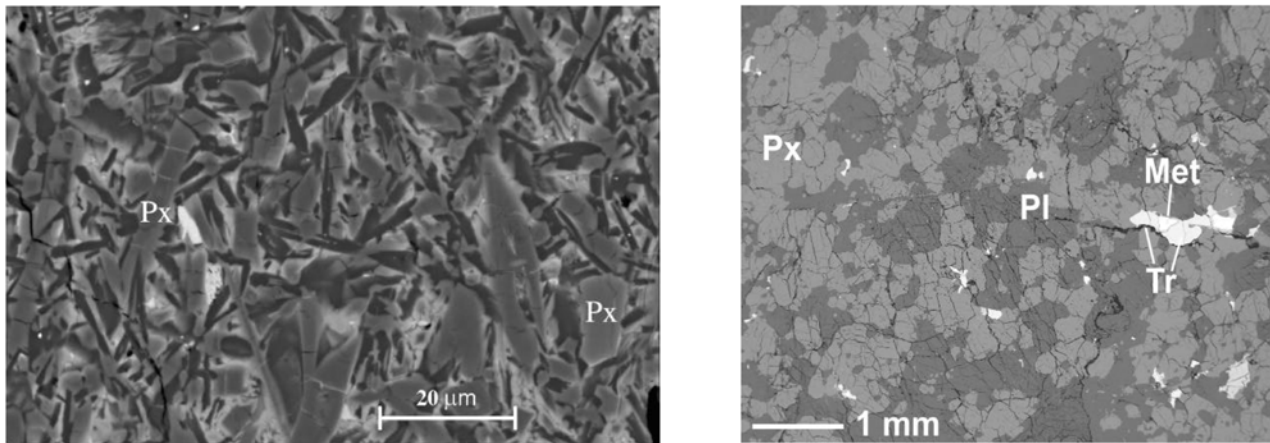


Fig. 3. a) Impact-melt vein in Dhofar 007: microporphyritic pyroxene crystals occur in an ophitic groundmass. A BSE image. b) The texture of a typical coarse-grained clast in Dhofar 007. A BSE image.

Dhofar 300 Samples

Ar Carrier Phases

To demonstrate the retentivity of Ar of specific minerals, the fractional release of Ar extracted by stepwise heating is shown against the degassing temperature in Fig. 4 for Dhofar 300. In the plagioclase separate (Fig 4b), both K-derived ^{39}Ar and Ca-derived ^{37}Ar degas simultaneously between 800 °C and 1500 °C, reflecting Ar released from the plagioclase lattice. Such broad release peaks of plagioclase were also observed in some plagioclase separates from howardites (Rajan et al. 1975; Rajan et al. 1979). The fluctuations of ^{39}Ar and ^{37}Ar release patterns could reflect chemical variations of plagioclase composition. Indeed, Dhofar 300 plagioclase compositions vary significantly (Table 1). Meanwhile, the K/Ca ratio is not so sensitive to such chemical variations and hardly changes (see below). There is a sharp peak at high temperatures around 1450 °C. Neither whole rock nor pyroxene samples display similar peaks, but the K/Ca ratio is identical to that in plagioclase. We consider that Ca-rich plagioclase can degas significant amounts of Ar at 1450 °C, which was previously demonstrated by Jessberger and Ostertag (1982) for a labradorite separate. In the whole rock sample of Dhofar 300, plagioclase degassing may have been facilitated due to eutectic melting at lower temperatures (~1320 °C) because of the presence of pyroxene. Moreover, the preferably picked large plagioclase grains of the separate could also enhance this phenomenon.

In the pyroxene separate (Fig. 4c), the ^{37}Ar release peak is dominated by Ca-bearing pyroxene degassing at high temperatures between 1100 °C and 1400 °C, as is commonly observed for terrestrial pyroxene (Trieloff et al. 1997) or extraterrestrial pyroxene (Trieloff et al. 2003; Pellas et al. 1997). We cannot observe release of K-derived ^{39}Ar correlating with the release of Ca-derived ^{37}Ar from the pyroxene lattice at high temperatures (>1200 °C). Rather, the ^{39}Ar release pattern is very similar to plagioclase. As some

small plagioclase grains could not be successfully removed from pyroxene grains, it is obvious that ^{39}Ar degasses from these plagioclase impurities. However, these dominate the K budget and hence the release spectrum and the age information. The K concentration of the pyroxene separate of 55 ppm when compared to the plagioclase with 767 ppm indicates about 7% plagioclase impurities (Table 2).

The whole rock release pattern (Fig. 4a) can be explained by a superposition of plagioclase and pyroxene release patterns, but does not have the high temperature phase observed in the plagioclase separate, for the reasons mentioned above.

All samples display distinct release peaks of trapped ^{36}Ar at 450 °C and 700 °C (Fig. 4). This trapped component is of atmospheric composition, as revealed by line fits to the low temperature extractions (generally <800 °C) in three-isotope correlation diagrams (Figs. 5a–c). For instance, the low temperature extractions of the plagioclase separate (Fig. 5b) yield an intercept of the $^{36}\text{Ar}/^{40}\text{Ar}$ ratio that closely matches the terrestrial atmospheric ratio of 0.00338. The whole rock sample and the pyroxene separate show similar correlations, though not as well defined. As all desert meteorites examined by us display this specific low temperature phase, we suggest a desert alteration product as the carrier of atmospheric Ar (see below).

^{40}Ar - ^{39}Ar Chronology

Figures 5d–f show the ^{40}Ar - ^{39}Ar age spectra of Dhofar 300 samples. If age spectra are not corrected for the atmospheric contamination revealed from the isochron diagrams (Figs. 5a–c), the low temperature extractions (first 10–20% of the fractional ^{39}Ar release) display high apparent ages up to 9 Ga, clearly exceeding the age of the solar system of 4.6 Ga. On the contrary, if low temperature extractions (up to 700 °C) are corrected for atmospheric ^{40}Ar (i.e. radiogenic Ar is calculated by subtracting atmospheric ^{40}Ar with $^{40}\text{Ar}/^{36}\text{Ar} = 295.5$ from total ^{40}Ar), the age spectra become more

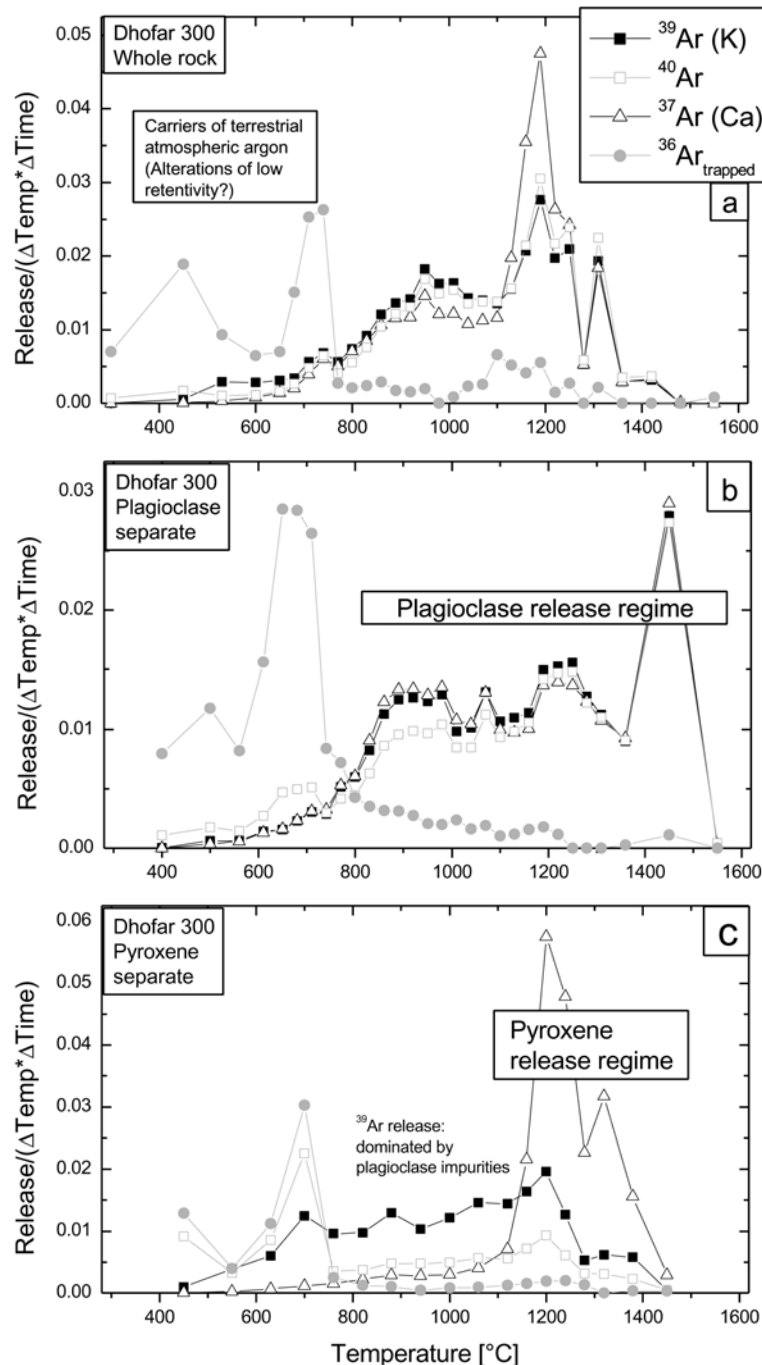


Fig. 4. Degassing pattern of argon isotopes of Dhofar 300 samples. All samples display distinct release peaks of trapped ^{36}Ar at $\sim 450^\circ\text{C}$ and $\sim 700^\circ\text{C}$. Pyroxene and plagioclase release regimes are indicated for mineral separates. The whole rock release pattern is a superposition of plagioclase and pyroxene release patterns.

similar to spectra of other non-desert eucrites, with stepwise increasing apparent ages.

Figure 6 shows all corrected ^{40}Ar - ^{39}Ar age and K/Ca spectra within a single diagram for comparison. The K/Ca ratio reflects the chemistry of the specific mineral phases. For the plagioclase separate, the K/Ca ratio is nearly constant and agrees with the K/Ca ratio measured by EMPA (Tables 1 and

2), except for some extractions at low temperatures with somewhat higher K/Ca ratios. In the whole rock and pyroxene spectrum, the K/Ca ratios at low extraction temperatures are even higher (up to a factor of 10). As these extractions are also contaminated by atmospheric Ar, the high K/Ca ratios indicate the respective carrier phase (presumably a desert alteration product). The K/Ca ratios of the pyroxene spectrum

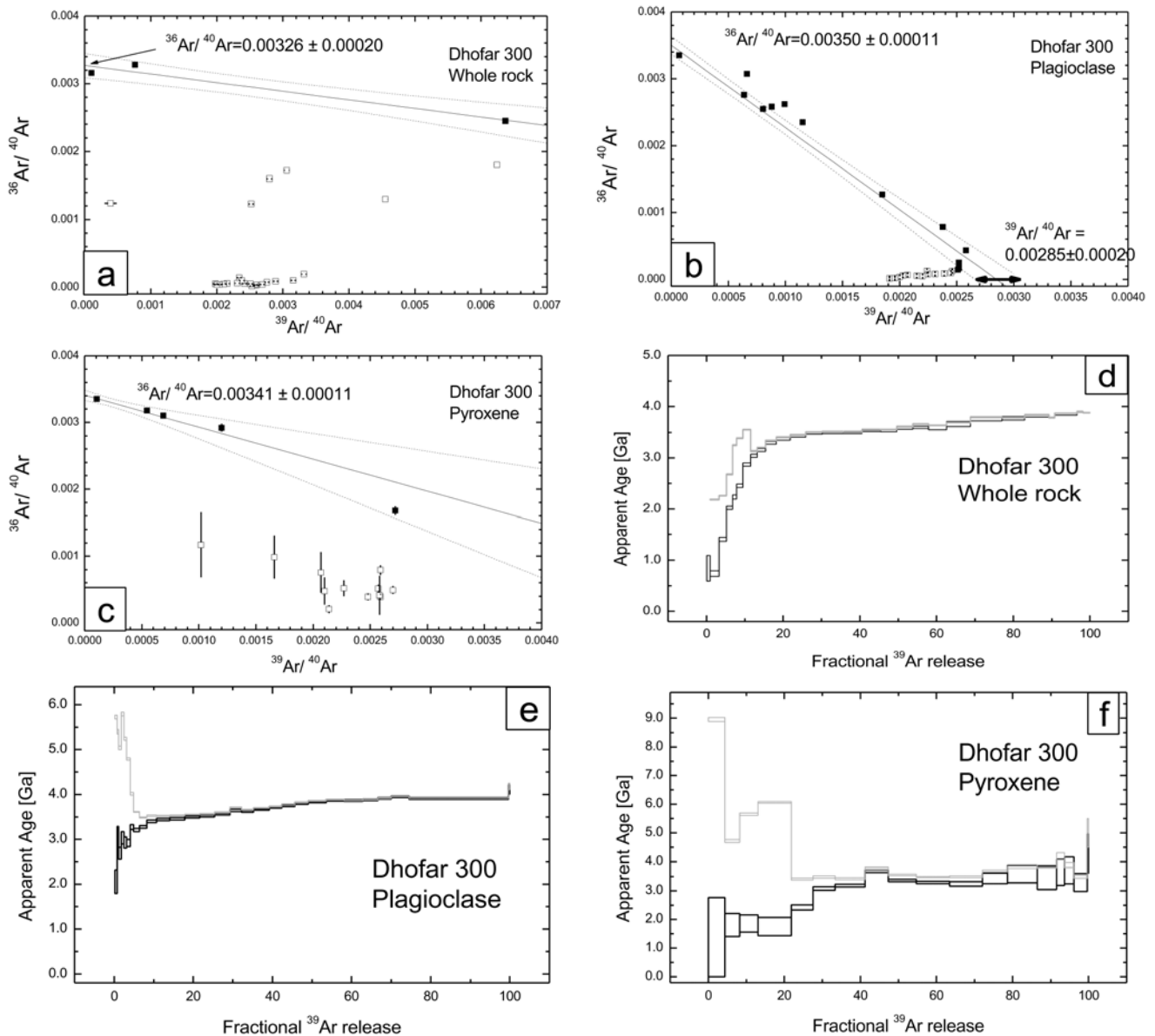


Fig. 5. a–c) Isochron plots with $^{36}\text{Ar}/^{40}\text{Ar}$ versus $^{39}\text{Ar}/^{40}\text{Ar}$ ratios for Dhofar 300 samples. The low temperature extractions (closed symbols) are linearly correlated pointing to a trapped Ar component with atmosphere-like $^{36}\text{Ar}/^{40}\text{Ar}$ ratios. Open symbols: high temperature extractions. d–f) Age spectra of Dhofar 300 samples. Correction of the low temperature extractions for air Ar results in more reasonable age spectra. High apparent ages exceeding the age of the solar system disappear.

decrease by a factor of >10 at high extraction temperatures, reflecting the above-mentioned degassing of ^{37}Ar derived from the pyroxene lattice. The intermediate part of the spectrum (30–60% of the fractional ^{39}Ar release) is associated with the degassing of plagioclase “impurities.” The K/Ca spectrum of the whole rock sample is more dominated by plagioclase grains, the main source of K, and degassing of pyroxene-derived ^{37}Ar only weakly influences the spectrum at high temperatures.

Regarding the degassing pattern and K/Ca spectra of plagioclase and pyroxene separates and the whole rock sample, we can conclude that the age information (corrected

for atmospheric contamination) is dominated by calcic plagioclase in all cases. Indeed, the age spectra are similar, having stepwise increasing apparent ages up to 4 Ga. Principally, this type of age spectra can be explained by a late (<1 Ga) thermal event that induced secondary ^{40}Ar loss. However, comparing the age spectra (Fig. 6), it is evident that ^{40}Ar was lost to varying degrees. The plagioclase separate was much less affected than the whole rock and pyroxene separate. This is most probably due to the different grain sizes of plagioclase in the three samples; for the plagioclase separate, preferably large plagioclase grains were picked ($\sim 800 \mu\text{m}$, see sample description). For the pyroxene

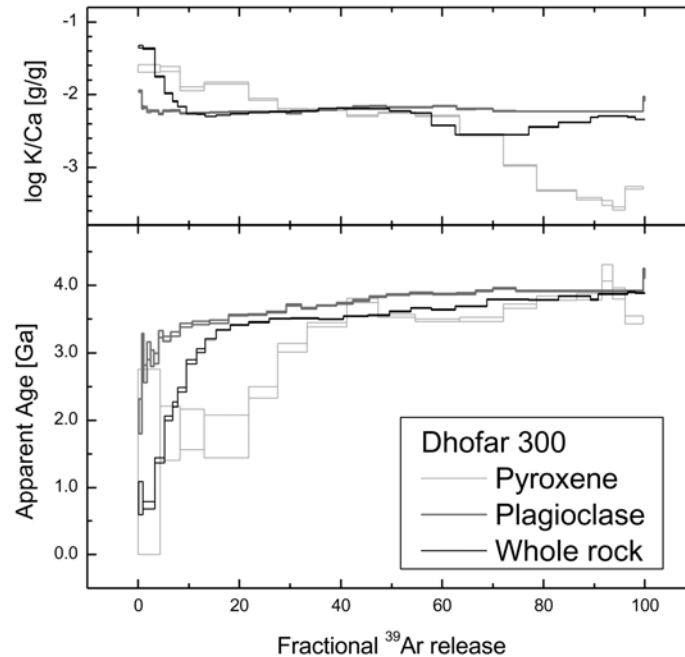


Fig. 6. K/Ca spectra and corrected age spectra of Dhofar 300 samples. Age spectra show various degree of secondary ^{40}Ar loss. The last total reset age is 3.9 ± 0.1 Ga for all samples.

separate, affected most strongly by the secondary ^{40}Ar loss, large plagioclase grains were avoided during handpicking, and the remaining plagioclase “impurities” (which control the pyroxene age spectrum) were inevitably more fine-grained (~ 300 μm or smaller, see sample description). The age spectrum of the whole rock sample, containing the original grain size distribution, is a superposition of plagioclase and pyroxene separate age spectra. Obviously, the response of various grain sizes to the recent thermal event is different, as the mineral’s ability to retain radiogenic ^{40}Ar during reheating depends on the mineral’s grain size. Another possible interpretation is that low apparent ages are to a certain extent due to K introduced during weathering (specifically, the proportion of K in excess of $\log(\text{K}/\text{Ca}) > -2.2$ in the K/Ca spectra).

Apparent ages of all samples in the high temperature extractions indicate that the last total reset occurred 3.9 ± 0.1 Ga ago, which is coeval with the intense cratering period on the Moon.

Dhofar 007 Samples

^{40}Ar - ^{39}Ar Chronology

Although Dhofar 007 is a cumulate eucrite, the Ar systematics has much in common with the Dhofar 300 noncumulate eucrite described above, displaying similar release patterns for plagioclase, pyroxene, and whole rock samples, and similar peaks of trapped ^{36}Ar occur at 450 $^{\circ}\text{C}$ and 700 $^{\circ}\text{C}$ with atmosphere-like $^{36}\text{Ar}/^{40}\text{Ar}$ ratios (see Appendix).

Correction of the low-temperature extractions for air Ar again results in more reasonable age spectra for plagioclase and whole rock samples (Fig. 7). The age spectrum of the whole rock sample is rather flat (Fig. 7), and, as in the case of Dhofar 300, the last total reset age is about 3.9 ± 0.2 Ga, which is coeval with the late lunar cratering period. The slowly rising apparent ages within the age spectrum of the whole rock sample may indicate either slow cooling or reheating 3.4 Ga ago. According to the release pattern of the plagioclase separate, its high temperature fractions were also corrected for the trapped component recognized by the three isotope correlation plot (Fig. A2b), because it could be due to an excessively high furnace blank or excess Ar incorporated during the last reset of the meteorite (e.g., Ar implanted by shock). However, the plagioclase age spectrum remains complicated (Fig. 7); apparent ages increase up to 4.5 Ga at high temperatures and persist even if we apply a correction for trapped Ar. Hence, we cannot exclude the presence of relict ^{40}Ar in more retentive or larger plagioclase grains. We note that apparent ages as high as 4.5 Ga commonly occur among the subgroup of cumulate eucrites (Bogard and Garrison 2003) consistent with the cumulate classification of Dhofar 007 (Afanasiev et al. 2000).

NWA 011

^{40}Ar - ^{39}Ar Chronology

The NWA 011 whole rock sample (Fig. A3) can be interpreted more easily based on the analyses of the Dhofar 300 and 007 mineral separates and whole rock samples.

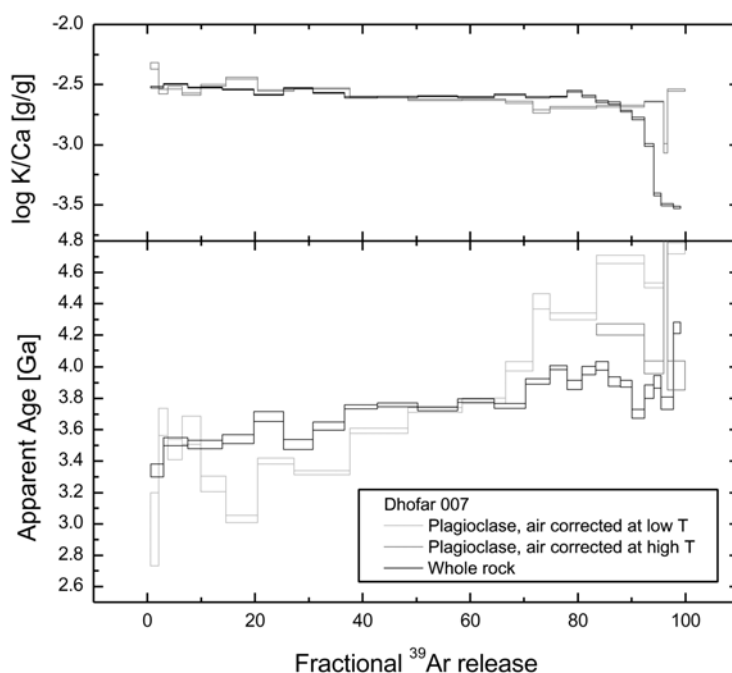


Fig. 7. K/Ca and corrected age spectra of Dhofar 007 whole rock and plagioclase separate. The plagioclase age spectrum has an undulating shape and an apparent ages increase up to 4.5 Ga at high extraction temperatures. The whole rock age spectrum is rather flat and shows that the last total reset occurred at about 3.9 ± 0.2 Ga ago.

Ortho- and clinopyroxene degas at high temperatures and plagioclase degas at intermediate temperatures, possibly together with phosphates and silica (Fig. A3). Similar to the Dhofar 300 and Dhofar 007 eucrites, there are peaks at low temperatures containing trapped Ar of atmospheric composition (three isotope correlation diagram in Fig. 8a), but also some K and in situ radiogenic Ar are present in the 700 °C peak. The age spectrum of NWA 011, when corrected for atmospheric Ar in the low temperature extractions, is similar to eucrite age spectra (Fig. 8b) as apparent ages generally increase with extraction temperature. Apparent ages of low temperature extractions indicate partial degassing <1.5 Ga ago. Maximum age values of ~3.9 Ga are observed at 60–70% of the fractional ^{39}Ar release, while for the last 25% of the ^{39}Ar release the apparent ages are considerably lower (close to 3.2 Ga). This feature persists, whether we correct high temperature extractions for atmospheric Ar or not. Such a correction could be indicated by the release of ^{36}Ar between 1200 °C and 1500 °C (Fig. A3) if this is due to an unrecognized, excessively high furnace blank.

Bogard and Garrison (2004) also presented NWA 011 age spectra of a whole rock sample and separated feldspar. The former sample was treated with an organic-based complexing agent and the latter was leached with dilute nitric acid etching before irradiation to reduce weathering products. Similar features of the whole rock age spectrum are ages of 3.1–3.2 Ga between 80% and 100% of the fractional ^{39}Ar release, preceded by significantly higher apparent ages between 50%

and 80% of the fractional ^{39}Ar release. However, Bogard and Garrison (2004) observed both lower K/Ca ratios and lower apparent ages in the first 10% of the fractional ^{39}Ar release, indicating successful removal of alterations by the complexing agent used for whole rock treating, dithionite citrate bicarbonate. However, for their feldspar sample, the treatment using HNO_3 was apparently less efficient, as shown by large excesses in the K/Ca ratio (up to 30–40% of the fractional ^{39}Ar release) and the presence of significant amounts of atmospheric Ar in low-temperature extractions. At high extraction temperatures, apparent ages close to 3.1–3.2 Ga were interpreted to most probably reflect the last total reset age, although this interpretation is not without problems; ages higher up to 3.9 Ga would then have to be attributed to excess ^{40}Ar introduced by weathering (Bogard and Garrison 2004) without being supported by ^{36}Ar , and it seems difficult to explain why the feldspar separate (with a high abundance of alterations) has no excess ages at high temperatures, contrary to the whole rock sample from which alterations were removed. Possible alternative explanations of excess ages as high as 3.9 Ga involve ^{39}Ar recoil losses (Huneke and Smith 1976; Turner and Cadogan 1974; Kunz et al. 1995) from the fine-grained feldspar fraction which is present in the whole rock. It could possibly lose recoiling ^{39}Ar into K-poor phases such as silica or phosphates degassing at intermediate temperatures. This effect would hardly occur in the separate containing large separated feldspar grains. Nevertheless, we also consider ^{39}Ar recoil redistribution not a completely satisfactory explanation.

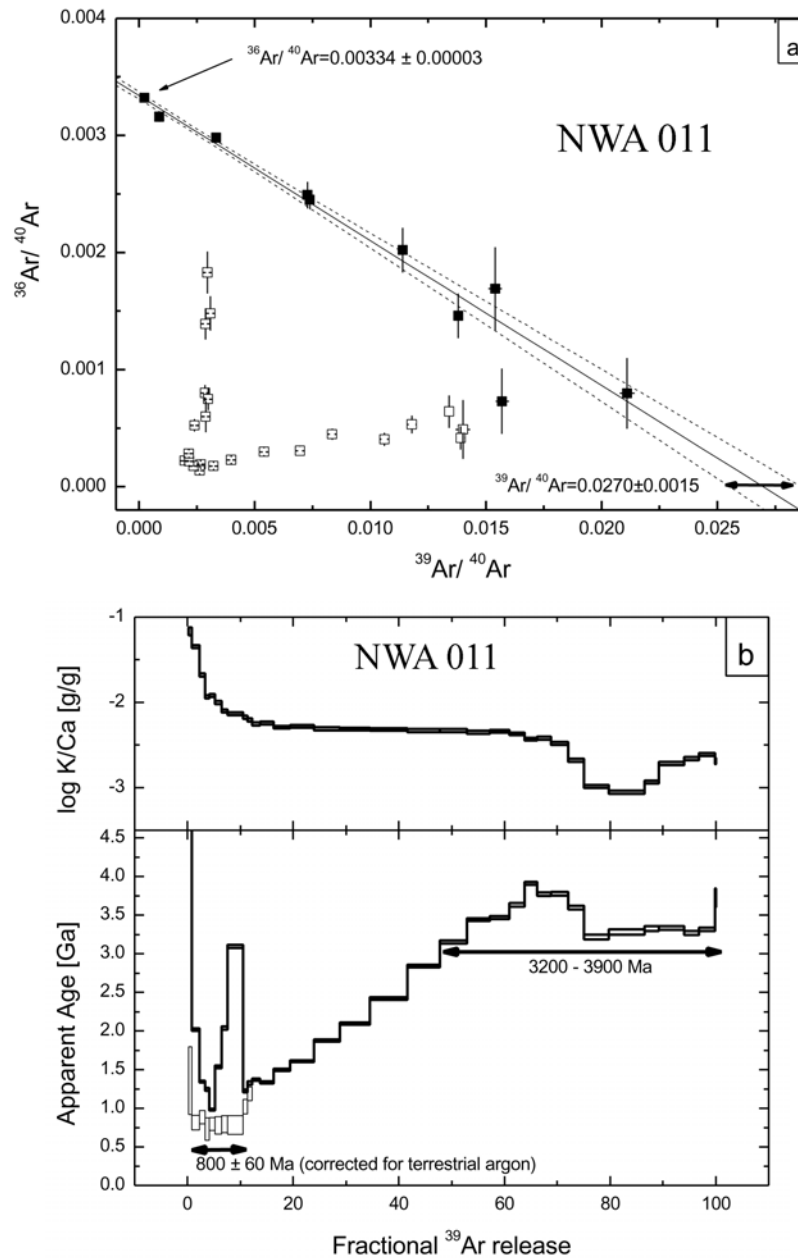


Fig. 8. a) Isochron plot of $^{36}\text{Ar}/^{40}\text{Ar}$ versus $^{39}\text{Ar}/^{40}\text{Ar}$ for NWA 011. Open/closed symbols: high/low temperature extractions. b) K/Ca spectrum and age spectrum of NWA 011 whole rock.

Last Total Reset ^{40}Ar - ^{39}Ar Ages of Dhofar 300, Dhofar 007, and NWA 011

The source reservoir of NWA 011 differentiated from its parent body at ~ 4563 Ma, approximately 4.7 Ma after fractionation of the NWA 011 parent body (Bogdanovski and Lugmair 2004). Nyquist et al. (2003) reported a ^{147}Sm - ^{143}Nd age of NWA 011 of 4.46 ± 0.04 Ga. The ^{40}Ar - ^{39}Ar age spectra indicate the last total reset of the K-Ar system between 3.2–3.9 Ga, which is most probably related to an impact event. Regarding ^{40}Ar - ^{39}Ar chronology, when compared with eucrites, a distinct chronology cannot be

inferred. Rather, the origin of NWA 011 from a different parent body must be deduced from oxygen isotopic composition and chemical arguments.

A last total reset ^{40}Ar - ^{39}Ar age of 3.9 Ga, as inferred for Dhofar 300 and possibly Dhofar 007, would be compatible with impact reset during the late heavy meteorite bombardment experienced by the Moon and also the HED parent body. Meanwhile, if a reset age of 3.1–3.3 Ga turned out to be valid for NWA 011, this would indicate that the NWA 011 parent body experienced a cratering activity unconnected with the “late lunar” bombardment. 3.1–3.3 Ga ago. Intense basaltic volcanism filling the lunar maria was

already active on the Moon and the impactor flux had dropped substantially after ~ 3.8 Ga ago. For Dhofar 007, the plagioclase high-temperature extractions could indicate a higher total reset age of 4.5 Ga, well within the typical age value of 4.48 ± 0.02 Ga of other cumulate eucrites (Bogard and Garrison 2003).

Atmospheric Contamination, Possible Alterations, and Significance of Low-Temperature Isochron Ages of Desert Meteorites

Up to now, we have not discussed the chronological significance of apparent isochrons formed by low temperature extractions. Such isochrons can be observed, more or less well defined, for all examined desert meteorites (Figs. 5a–c, 8a, and A2a–d), and in all cases the trapped Ar component is of atmospheric composition released in two characteristic peaks at 450 °C and 700 °C (Figs. 4, A1, and A3). This component is also present in mineral separates and is sometimes associated with relatively high K/Ca ratios. These features suggest a relation to alteration products that also influence other geochemical tracers (Stelzner et al. 1999).

Particularly for NWA 011, an isochron analysis at low temperatures shows a highly linear array (Fig. 8a). Correction of the respective extractions for trapped Ar of atmospheric composition yields a partial plateau with an age of 0.80 ± 0.06 Ga (Fig. 8b). For the Dhofar meteorites, low temperature isochrons (Figs. 5b, 5c, A2b, and A2c) of plagioclase and pyroxene separates yield ages of 3.0 ± 0.2 and 1.8 ± 0.5 Ga for Dhofar 300, and 3.4 ± 0.2 and ~ 2.0 Ga for Dhofar 007, respectively, that also can be identified as small partial age plateaus in the age spectra (Figs. 6 and 7). As the plateau age values within a single meteorite are clearly inconsistent, we conclude that they are not chronologically relevant, but rather are artifacts due to terrestrial weathering. Possible alteration products carrying atmospheric Ar in these meteorites are Fe-rich oxides replacing metal and troilite, terrestrial quartz and carbonates, Ba sulfate filled cracks, and mineral fractures. However, all these alteration products do not contain significant amounts of K, though some ^{39}Ar degasses at low temperatures. Possible K-bearing alterations are clays or salts, which could have formed from colloid or simple solutions penetrating through cracks or fissures.

As apparent ages in low temperature extractions are similar to the low age end of the horizontal array of data formed by the high temperature steps (Figs. 5b and 8a), this appears to suggest mixing of air from weathering products and partial release from grain boundaries of plagioclase grains. However, the observation that low temperature extractions form partial plateaus needs some kind of homogenization of ^{40}Ar and K in grain boundaries affected by weathering. Thus, we tentatively suggest that during weathering and alteration of meteorite minerals there is an equilibration of: i) K and radiogenic ^{40}Ar from the meteorite

(probably from plagioclase grain boundaries) and ii) occasionally K-induced from the desert environment. While the first effect (equilibration) causes low-temperature age plateaus, the second effect should lower the respective plateau age and increase the K/Ca ratio, which is actually observed for Dhofar 300 pyroxene when compared to Dhofar 300 plagioclase (Fig. 6).

Another effect of desert weathering is the incorporation of atmospheric Ar, but our observations also indicate additional air contamination during laboratory handling. Surprisingly, Dhofar 300 and Dhofar 007 whole rock samples contain relatively low abundances of trapped atmospheric ^{36}Ar and ^{38}Ar when compared to the respective mineral separates (Table 2). Crushing during mineral separation or washing could be the reasons of additional atmospheric contamination of monomineralic samples, as indicated by previous studies. Niemeyer and Leich (1976) showed that sample crushing to fine grain sizes yielded an order-of-magnitude increase of trapped noble gases. Niedermann and Eugster (1992) reported a correlation of grain size and concentrations of trapped atmospheric noble gases for grain sizes of ≤ 30 μm , indicating that fresh grain surfaces prepared during crushing can trap significant amounts of atmospheric Ar. However, as atmospheric Ar is released from all samples at the same temperature (Figs. 4, A1, and A3), incorporation must have occurred into specific low-temperature phases preferably. For Dhofar 300 and Dhofar 007 samples, there is a trend of increasing contents of trapped atmospheric Ar in the sequence, whole rock-pyroxene-plagioclase-glass (Table 2). This reflects the total contamination process during both desert residence and sample preparation.

Cosmic-Ray Exposure Ages

To calculate cosmic-ray exposure (CRE) ages, we employed cosmogenic ^{38}Ar , which is the total ^{38}Ar corrected for trapped ^{38}Ar and, in some cases, for Cl-derived ^{38}Ar . Table 2 presents the calculated abundances of trapped, Cl-derived, and cosmogenic ^{38}Ar . While the value for the latter component is an upper limit, values for Cl-derived and trapped components are lower limits. As the $^{36}\text{Ar}/^{38}\text{Ar}$ ratios are higher than 0.65 in each Ar extraction of plagioclase and pyroxene separates of Dhofar 300 and NWA 011, the presence of Cl-derived ^{38}Ar is not compelling. Indeed phosphates, the main source of Cl in Dhofar 300, are very rare and distributed unevenly. Possible Cl-bearing terrestrial contaminants are not important, as the low-temperature extractions are not taken into account for the calculation of exposure age spectra.

The CRE ages of Dhofar 300 and Dhofar 007 are presented as stepwise release age spectra. Since whole rock sample exposure age spectra are complicated due to their multiphase nature and the inhomogeneous distribution of the

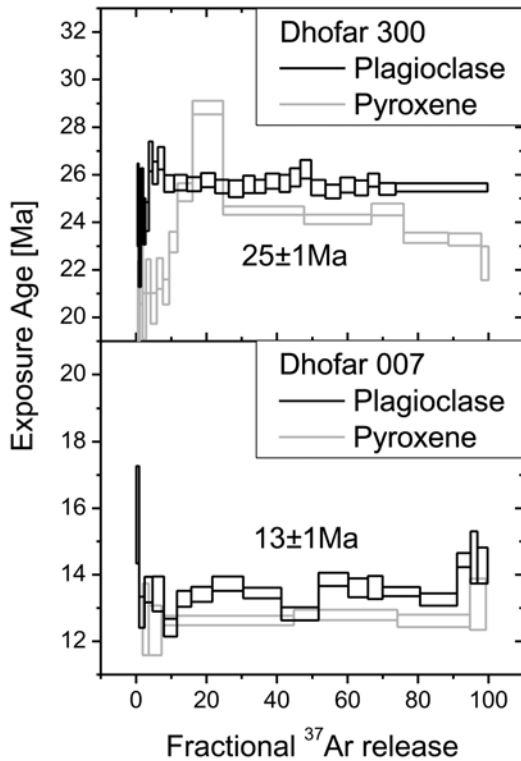


Fig. 9. CRE age spectra of mineral separates of Dhofar 300 and Dhofar 007. Pyroxene and plagioclase exposure age spectra were calculated with the mineral specific target element chemistry and corresponding production rates of cosmogenic ^{38}Ar , and are highly concordant.

target elements (e.g., different Fe/Ca ratios of plagioclase and pyroxene), we use exposure age spectra of mineral separates only. For monomineralic samples, we can expect a coherent degassing of cosmogenic ^{38}Ar related to different target elements such as Ca and Fe in pyroxene because both are lattice elements in this mineral. The advantage of this presentation mode is that the CRE age is estimated by plateau fractions of the sample; ages of extractions distorted by the presence of reactor-derived $^{38}\text{Ar}_{\text{Cl}}$ or by possible loss caused by solar heating or weathering can be excluded. Meanwhile, in contrast to Ar-Ar age spectra, the largest uncertainty in deriving a CRE age, beyond uncertainties in determining cosmogenic Ar concentrations, is in adopting a production rate that varies with composition and shielding. Such uncertainties are not taken into account by age error boxes of the CRE age spectrum. However, uncertainties in production rates depending on chemical composition are reflected by systematic differences of age spectra of minerals such as plagioclase and pyroxene, because their composition and production rates differ significantly (see below). To plot CRE age spectra, we applied the following procedure. For each extraction of Dhofar 300 and Dhofar 007 samples, cosmogenic ^{38}Ar was normalized to the Ca concentration determined from ^{37}Ar . Production rates for cosmogenic ^{38}Ar

were individually calculated for plagioclase and pyroxene monomineralic samples of Dhofar 300 and Dhofar 007 using the measured chemical composition of these phases (Table 1) according to the method by Eugster and Michel (1995). The contributions from all target elements recommended by Eugster and Michel (1995), Ca, Fe, Ni, Ti, Cr, Mn, and K, were taken into account. Then, production rates were normalized to the Ca concentration of the respective mineral phase. Calculated ^{38}Ar production rates, in units of $10^{-10} \text{ cm}^3 \text{ STP/g per Ma} \times \text{Ca}$ are 2.30 and 1.81 for Dhofar 300 pyroxene and plagioclase, respectively, and 2.57 and 1.82 for Dhofar 007 pyroxene and plagioclase, respectively. Shielding correction was not applied to the production rate of cosmogenic ^{38}Ar . Although Reedy and Kim (2004) recommend such a correction, Wakefield et al. (2004) have demonstrated that it is negligible for eucrites.

Dhofar 300 and Dhofar 007 CRE ages were plotted versus the fraction of Ca-derived ^{37}Ar released (Fig. 9). Uncertainties include analytical precision only. Due to the higher number of plateau fractions of plagioclase, and the fact that Ca accounts for >95% of the cosmogenic ^{38}Ar , we consider the values obtained from plagioclase as far more reliable than the pyroxene spectra. For pyroxene, a major problem arises from the contributions of high-Ca and low-Ca pyroxene, that is difficult to quantify exactly. This parameter is important because the two pyroxenes have different Ca/Fe ratios and Fe contributes a significant proportion of cosmogenic ^{38}Ar (up to 25%). Nevertheless, though the very different contributions from Fe-derived ^{38}Ar and the different Ca-normalized production rates applied, pyroxene and plagioclase exposure age spectra are highly concordant. We determine an exposure age of $25 \pm 1 \text{ Ma}$ for Dhofar 300 and of $13 \pm 1 \text{ Ma}$ for Dhofar 007 (Fig. 9). These values represent the average exposure ages of plagioclase and pyroxene separates, and uncertainties take into account their variability.

These exposure ages are within the range of the values reported for eucrites ranging from 5 to 80 Ma, and the Dhofar 300 exposure age agrees with one of two statistically significant clusters of exposure ages at 20–25 and 35–42 Ma (Eugster and Michel 1995; Welten et al. 1997). Eugster and Michel (1995) also noted less pronounced minor clusters, one of them at $12 \pm 2 \text{ Ma}$, consistent with the exposure age of Dhofar 007. Moreover, Wakefield et al. (2004) have recently studied the exposure ages of several cumulate and unbrecciated eucrites and some of these ages are ~12–16 Ma (Wakefield et al. 2004). Such a clustering of HED CRE ages is one of the fundamental arguments that might indicate derivation from a limited region of their parent asteroid (Mittlefehldt 2004).

The CRE age of NWA 011 was calculated based on the total amount of cosmogenic ^{38}Ar and production rate determined for whole rock employing the above mentioned method and chemical composition of Korochantseva et al. (2003). Unlike a stepped release plot, such a calculation

would not be subject to uncertainties about which phases are releasing cosmogenic Ar. The evaluated production rate of ^{38}Ar for NWA 011 is $15.83 \times 10^{-10} \text{ cm}^3 \text{ STP/g per Ma}$. The calculated CRE age of $\sim 28 \text{ Ma}$ is a little bit higher than the age of $\sim 25 \text{ Ma}$ reported previously (Bogard and Garrison 2004). Yamaguchi et al. (2002) presented several exposure ages, determined from cosmogenic ^3He , ^{21}Ne , and ^{38}Ar , which are 11, 30, and 23 Ma, and also the ^{81}Kr -Kr age of $39 \pm 5 \text{ Ma}$. They suggest that the shorter ages from ^3He and ^{38}Ar probably come from partial loss of these gases by terrestrial weathering and that the ^{81}Kr -Kr age is an upper limit. Our CRE age is similar to the ^{21}Ne -derived exposure age. The exposure age of NWA 011 is also close to the two major peaks of HED exposure ages (Eugster and Michel 1995; Welten et al. 1997). Having the exposure age of a single sample from the NWA 011 parent body, it is unclear whether this coincidence is statistically meaningful or not.

SUMMARY AND CONCLUSIONS

Dhofar 300 is a brecciated noncumulate eucrite (Grossman and Zipfel 2001). The last total reset of its K-Ar system occurred $\sim 3.9 \text{ Ga}$ ago, which is commonly observed for other brecciated noncumulate eucrites reset by impact and coincides with the period of enhanced cratering activity on the Moon. Dhofar 300 is not heavily shocked, which indicates that shock metamorphism did not reset the K-Ar system, in agreement with previous experimental observations on Carich plagioclase (Jessberger and Ostertag 1982). Equilibration of pyroxenes and the clouded appearance of silicate minerals demonstrate that Dhofar 300 was affected by thermal metamorphism, possibly by tempering effects accompanying a 3.9 Ga impact event.

Dhofar 007 is a brecciated, cumulate eucrite (Afanasyev et al. 2000) strongly enriched in FeNi metal and siderophiles (Yamaguchi et al. 2003). We infer an upper age limit of 4.5 Ga, closely resembling the age value of $4.48 \pm 0.02 \text{ Ga}$ of other cumulate eucrites (Bogard and Garrison 2003). This age has been interpreted to be an age of the impact event excavating cumulate (and some non-cumulate) eucrites, unconnected with the original eucrite differentiation and cooling event that must have taken place a few Ma after Allende CAIs. The high abundance of FeNi metal and high concentrations of siderophile elements in some clasts of this meteorite can be explained by the admixture of chondritic projectile material (Yamaguchi et al. 2003). Contamination by a chondritic component has been earlier demonstrated for three Pasamonte clasts by Metzler et al. (1995). The mixing of indigenous eucrite material and siderophile-rich impact lithologies was caused either by the same impact that excavated and reset Dhofar 007 and other cumulate eucrites $\sim 4.5 \text{ Ga}$ ago or by an earlier impact event.

Impact resetting of NWA 011 took place during the time period of ~ 3.2 – 3.9 Ga ago. As there is no final agreement about the age spectrum and exact age of NWA 011, neither a

clear-cut difference to eucrite chronologies can be inferred, nor an impact reset that would be apart from the late heavy bombardment affecting the Moon.

Partial degassing events affected the K-Ar system of our studied meteorites subsequently similar to other eucrites about 3.4 Ga ago for Dhofar 007, and $<1.5 \text{ Ga}$ ago for Dhofar 300 and NWA 011. The Dhofar 007 impact melt veins discordantly intersecting the meteorite are most probably the result of a late event, when Dhofar 007 was already a breccia. Partial age plateaus or isochrons defined by low-temperature extractions of Dhofar 300, Dhofar 007, and NWA 011 do not represent chronologically meaningful events and are most likely not suitable to reconstruct such events. Cosmic-ray exposure ages of Dhofar 300 and Dhofar 007 are $25 \pm 1 \text{ Ma}$ and $13 \pm 1 \text{ Ma}$, respectively. They agree with the established exposure age clusters for HED meteorites. The CRE age of NWA 011 is $\sim 28 \text{ Ma}$.

Applying stepwise heating ^{40}Ar - ^{39}Ar analyses using a large number of thermal extractions resulted in highly resolved age spectra on different monomineralic separates and allows some methodological conclusions:

1. It was possible to reasonably interpret mineral release patterns and to identify one or two minor carrier phases in all samples, most probably desert alterations, which release atmospheric Ar at distinct temperatures of 450°C and 700°C . High-resolution step heating served to better resolve air contamination from the in situ radiogenic ^{40}Ar component, and respective corrections resulted in more plausible age spectra.
2. We infer that the low-temperature release of atmospheric Ar at $\sim 450^\circ$ and $\sim 700^\circ \text{C}$ is a typical feature of desert meteorites and is almost certainly related to alteration products. In addition, terrestrial residence seems to cause equilibration of K and accumulated radiogenic ^{40}Ar from the meteorite and occasionally K induced from the desert environment. This results in the formation of low-temperature “plateau” ages and isochrons.
3. Crushing during mineral separation and possible subsequent cleaning cause additional significant contamination by atmospheric Ar; all mineral separates contain higher abundances of trapped atmospheric ^{36}Ar and ^{38}Ar in comparison with the respective whole rocks. The content of trapped atmospheric Ar increases in the sequence, whole rock-pyroxene-plagioclase-glass.
4. Two important points are indicated by comparison of mineral separates and whole-rock ^{40}Ar - ^{39}Ar age spectra. The first is that the chronological information of whole rock and pyroxene separates is controlled by the plagioclase grains and plagioclase impurities. This resulted in no significant age difference of the last total reset age between whole rock, feldspar, and pyroxene separates observed for Dhofar 300. The statement that “pyroxene must be older, as pyroxene is more retentive” is fallacious. The second point is that the degree of secondary ^{40}Ar loss depends on mineral grain sizes.

Acknowledgments—We appreciate helpful discussions with E. K. Jessberger, and W. H. Schwarz. L. D. Barsukova is thanked for providing bulk compositions for Dhofar 300 and Dhofar 007. The manuscript benefitted from comments by M. A. Nazarov and M. A. Ivanova. We thank C. A. Lorenz and D. D. Badjukov for their participation in this study and access to their data. Reviews by D. D. Bogard, R. Burgess, U. Ott, and the editorial assistance of U. Riller helped substantially to improve the quality of this manuscript. We thank the Forschungszentrum Geesthacht (GKSS) for access to neutron irradiation facilities. E. V. Korochantseva, A. I. Buikin, and M. Trieloff acknowledge support by the Deutsche Forschungsgemeinschaft via grant TR333/3 and 4, 436 RUS 17/100/02, and 436 RUS 17/91/01.

Editorial Handling—Dr. Ulrich Riller

REFERENCES

- Afanasiev S. V., Ivanova M. A., Korochantsev A. V., Kononkova N. N., and Nazarov M. A. 2000. Dhofar 007 and Northwest Africa 011: Two new eucrites of different types (abstract). *Meteoritics & Planetary Science* 35:A19.
- Baldwin R. B. 1974. Was there a “terminal lunar cataclysm” 3.9–4.0 × 10⁹ years ago? *Icarus* 23:157–166.
- Boesenberg J. S. 2003. An oxygen isotope mixing model for the Northwest Africa 011 basaltic achondrite (abstract #1239). 34th Lunar and Planetary Science Conference. CD-ROM.
- Bogard D. D. 1995. Impact ages of meteorites: A synthesis. *Meteoritics* 30:244–268.
- Bogard D. D. and Garrison D. H. 2003. ³⁹Ar–⁴⁰Ar ages of eucrites and thermal history of asteroid Vesta. *Meteoritics & Planetary Science* 38:669–710.
- Bogard D. D. and Garrison D. H. 2004. ³⁹Ar–⁴⁰Ar dating of unusual eucrite NWA 011: Is it from Vesta? (abstract #1094). 35th Lunar and Planetary Science Conference. CD-ROM.
- Bogdanovski O. and Lugmair G. W. 2004. Manganese-chromium isotope systematics of basaltic achondrite Northwest Africa 011 (abstract #1715). 35th Lunar and Planetary Science Conference. CD-ROM.
- Brereton N. R. 1970. Corrections for interfering isotopes in the ⁴⁰Ar/³⁹Ar dating method. *Earth and Planetary Science Letters* 8:427–433.
- Grieve R. A. F and Cintala M. J. 1992. An analysis of differential impact-melt crater scaling and implications for the terrestrial impact record. *Meteoritics* 27:526–538.
- Grossman J. N. and Zipfel J. 2001. The Meteoritical Bulletin, No. 85. *Meteoritics & Planetary Science* 36:A293–A322.
- Eugster O. and Michel Th. 1995. Common asteroid breakup events of eucrites, diogenites, and howardites and cosmic-ray production rates for noble gases in achondrites. *Geochimica et Cosmochimica Acta* 59:177–199.
- French B. M. 1998. *Traces of catastrophe: A handbook of shock-metamorphic effects in terrestrial meteorite impact structures*. LPI Contribution #954. Houston, Texas: Lunar and Planetary Institute. 120 p.
- Harlow G. E. and Klimentidis R. 1980. Clouding of pyroxene and plagioclase in eucrites: Implications for post-crystallization processing. Proceedings, 11th Lunar and Planetary Science Conference. pp. 1131–1143.
- Hartmann W. K. 1975. Lunar “cataclysm”: A misconception? *Icarus* 24:181–187.
- Huneke J. C. and Smith S. P. 1976. The realities of recoil: ³⁹Ar recoil out of small grains and anomalous patterns in ³⁹Ar–⁴⁰Ar dating. Proceedings, 7th Lunar Science Conference. pp. 1987–2008.
- Jessberger E. K. 1982. The ⁴⁰Ar–³⁹Ar dating technique: Principles, developments, and applications in cosmochronology. *Chemie der Erde* 41:40–94.
- Jessberger E. K. and Ostertag R. 1982. Shock effects on the K–Ar system of plagioclase feldspar and the age of anorthosite inclusions from northeastern Minnesota. *Geochimica et Cosmochimica Acta* 46:1465–1471.
- Jessberger E. K., Dominik B., Staudacher Th., and Herzog G. F. 1980. ⁴⁰Ar–³⁹Ar ages of Allende. *Icarus* 42:380–405.
- Kaneoka I., Ozima M., and Yanagisawa M. 1979. ⁴⁰Ar–³⁹Ar age studies of four Yamato-74 meteorites. *Proceedings of the Third Symposium on Antarctic Meteorites* 12:186–206.
- Kaneoka I., Nagao K., Yamaguchi A., and Takeda H. 1995. ⁴⁰Ar–³⁹Ar analyses of Juvinas fragments. *Proceedings of the NIPR Symposium on Antarctic Meteorites*. pp. 287–296.
- Korochantseva E. V., Ivanova M. A., Lorenz C. A., Bouikine A. I., Trieloff M., Nazarov M. A., Promprated P., Anand M., and Taylor L. A. 2003. Major and trace element chemistry and Ar–Ar age of the NWA 011 achondrite (abstract #1575). 34th Lunar and Planetary Science Conference. CD-ROM.
- Kunz J., Trieloff M., Bobe K. D., Metzler K., Stöffler D., and Jessberger E. K. 1995. The collisional history of the HED parent body inferred from ⁴⁰Ar–³⁹Ar ages of eucrites. *Planetary and Space Science* 43:527–543.
- Melosh H. J. 1989. *Impact cratering: A geologic process*. New York: Oxford University Press. 245 p.
- Metzler K., Bobe K. D., Palme H., Spettel B., and Stöffler D. 1995. Thermal and impact metamorphism on the HED parent asteroid. *Planetary and Space Science* 43:499–525.
- Mittlefehldt D. W. 2004. The dichotomous HED meteorite suite (abstract #1553). 35th Lunar and Planetary Science Conference. CD-ROM.
- Niedermann S. and Eugster O. 1992. Noble gases in lunar anorthositic rocks 60018 and 65315—Acquisition of terrestrial krypton and xenon indicating an irreversible adsorption process. *Geochimica et Cosmochimica Acta* 56:493–509.
- Niemeyer S. and Leich D. A. 1976. Atmospheric rare gases in lunar rock 60015. Proceedings, 7th Lunar Science Conference. pp. 587–597.
- Nyquist L. E., Shih C.-Y., Wiesmann H., Yamaguchi A., and Misawa A. 2003. Early volcanism on the NWA 011 parent body (abstract). *Meteoritics & Planetary Science* 38:A59.
- Palme H. 2002. A new solar system basalt. *Science* 296:271–273.
- Pellas P., Fieni C., Trieloff M., and Jessberger E. K. 1997. The cooling history of the Acapulco meteorite as recorded by the ²⁴⁴Pu and ⁴⁰Ar–³⁹Ar chronometers. *Geochimica et Cosmochimica Acta* 61:3477–3501.
- Podosek F. A. and Huneke J. C. 1973. ⁴⁰Ar–³⁹Ar chronology of four calcium-rich achondrites. *Geochimica et Cosmochimica Acta* 37:667–684.
- Promprated P., Taylor L. A., Anand M., Rumble D., III., Korochantseva E. V., Ivanova M. A., Lorentz C. A., and Nazarov M. A. 2003. Petrology and oxygen isotopic compositions of anomalous achondrite NWA 011 (abstract #1757). 34th Lunar and Planetary Science Conference. CD-ROM.
- Rajan R. S., Huneke J. C., Smith S. P., and Wasserburg G. J. 1975. ⁴⁰Ar–³⁹Ar chronology of isolated phases from Bununu and Malvern howardites. *Earth and Planetary Science Letters* 27:181–190.
- Rajan R. S., Huneke J. C., Smith S. P. and Wasserburg G. J. 1979. ⁴⁰Ar–³⁹Ar chronology of lithic clasts from the Kapoeta howardite. *Geochimica et Cosmochimica Acta* 43:957–971.

- Reedy R. C. and Kim K. J. 2004. Production rates for noble-gas isotopes in eucrites (abstract #1357). 35th Lunar and Planetary Science Conference. CD-ROM.
- Ryder G. 1990. Lunar samples, lunar accretion, and the early bombardment of the Moon. *Eos* 71:322–323.
- Ruzicka A., Snyder G. A., and Taylor L. A. 1997. Vesta as the HED parent body: Implications for the size of a core and for large-scale differentiation. *Meteoritics & Planetary Science* 32:825–840.
- Schaeffer G. A. and Schaeffer O. A. 1977. ^{40}Ar - ^{39}Ar ages of lunar rocks. Proceedings, 8th Lunar Science Conference. pp. 2253–2300.
- Steiger R. H. and Jäger E. 1977. Subcommission on geochronology: Convention on the use of decay constants in geo- and cosmochronology. *Earth and Planetary Science Letters* 36:359–362.
- Stelzner Th., Heide K., Bischoff A., Weber D., Scherer P., Schultz L., Happel M., Schrön W., Neupert U., Michel R., Clayton R. N., Mayeda T. K., Bonani G., Haidas I., Ivy-Ochs S., and Suter M. 1999. An interdisciplinary study of weathering effects in ordinary chondrites from the Acfer region, Algeria. *Meteoritics & Planetary Science* 34:787–794.
- Stöffler D. and Ryder G. 2001. Stratigraphy and isotope ages of lunar geologic units: Chronological standard for the inner solar system. *Space Science Reviews* 96:9–54.
- Stöffler D., Keil K., and Scott E. R. D. 1991. Shock metamorphism of ordinary chondrites. *Geochimica et Cosmochimica Acta* 55:3845–3867.
- Takeda H., Mori H., and Bogard D. D. 1994. Mineralogy and ^{39}Ar - ^{40}Ar age of an old pristine basalt: Thermal history of the HED parent body. *Earth and Planetary Science Letters* 122:183–194.
- Tera F., Papanastassiou D. A., and Wasserburg G. J. 1974. Isotopic evidence for a terminal lunar cataclysm. *Earth and Planetary Science Letters* 22:1–21.
- Trieloff M., Reimold W. U., Kunz J., Boer R. H., and Jessberger E. K. 1994. ^{40}Ar - ^{39}Ar thermochronology of pseudotachylite at the Ventersdorp Contact Reef, Witwatersrand Basin. *South African Journal of Geology* 97:365–384.
- Trieloff M., Weber H. W., Kurat G., Jessberger E. K., and Janicke J. 1997. Noble gases, their carrier phases, and Ar chronology of upper mantle rocks from Zabargad Island, Red Sea. *Geochimica et Cosmochimica Acta* 61:5065–5088.
- Trieloff M., Deutsch A., and Jessberger E. K. 1998. The age of the Kara impact structure, Russia. *Meteoritics & Planetary Science* 33:361–372.
- Trieloff M., Jessberger E. K., Herrwerth I., Hopp J., Fiéni C., Ghélis M., Bourot-Denise M., and Pellas P. 2003. Structure and thermal history of the H chondrite parent asteroid revealed by thermochronometry. *Nature* 422:502–506.
- Turner G. 1971. ^{40}Ar - ^{39}Ar dating: The optimization of irradiation parameters. *Earth and Planetary Science Letters* 10:227–234.
- Turner G. 1977. Potassium-argon chronology of the Moon. *Physics and Chemistry of the Earth* 10:145–195.
- Turner G. and Cadogan P. H. 1974. Possible effects of ^{39}Ar recoil in ^{40}Ar - ^{39}Ar dating. Proceedings, 5th Lunar Science Conference. pp. 1601–1615.
- Turner G., Knott S. F., Ash R. D., and Gilmour J. D. 1997. Ar-Ar chronology of the Martian meteorite ALH 84001: Evidence for the timing of the early bombardment of Mars. *Geochimica et Cosmochimica Acta* 61:3835–3850.
- Wakefield K., Bogard D., and Garrison D. 2004. Cosmic-ray exposure ages, Ar-Ar ages, and the origin and history of eucrites (abstract #1020). 35th Lunar and Planetary Science Conference. CD-ROM.
- Warren P. H. and Jerde E. A. 1987. Composition and origin of Nuevo Laredo trend eucrites. *Geochimica et Cosmochimica Acta* 51:713–725.
- Warren P. H., Jerde E. A., Migdisova L. F., and Yaroshevsky A. A. 1990. Pomozdino: An anomalous, high-MgO/FeO, yet REE-rich eucrite. Proceedings, 20th Lunar and Planetary Science Conference. pp. 281–297.
- Welten K. C., Lindner L., van der Borg K., Loeken T., Scherer P., and Schultz L. 1997. Cosmic-ray exposure ages of diogenites and the recent collisional history of the HED parent body/bodies. *Meteoritics & Planetary Science* 32:891–902.
- Yamaguchi A., Clayton R. N., Mayeda T. K., Ebihara M., Oura Y., Miura Y. N., Haramura H., Misawa K., Kojima H., and Nagao K. 2002. A new source of basaltic meteorites inferred from Northwest Africa 011. *Science* 296:334–336.
- Yamaguchi A., Setoyanagi T., and Ebihara M. 2003. An anomalous eucrite, Dhofar 007, and a possible genetic relationship with mesosiderites (abstract #1377). 34th Lunar and Planetary Science Conference. CD-ROM.

APPENDIX

Dhofar 007 Ar Carrier Phases and Correction for Atmospheric Component

Although Dhofar 007 is a cumulate eucrite, the Ar systematics has much in common with the above described Dhofar 300 noncumulate eucrite. The Ar release patterns of Dhofar 007 samples are shown in Figs. A1a–d. In the plagioclase separate, the release of K-derived ^{39}Ar and Ca-derived ^{37}Ar at intermediate temperatures is related to argon from the plagioclase lattice (Fig. A1b). Plagioclase in Dhofar 007 is of a restricted composition (Table 1) and the fluctuations of the ^{39}Ar and ^{37}Ar release pattern are not as complex as observed in Dhofar 300. The K/Ca ratio is quite homogeneous (see below). In the case of the pyroxene separate (Fig. A1c), the high temperature peak of ^{37}Ar is dominated by Ar from the pyroxene lattice, while ^{39}Ar

degasses mostly from plagioclase impurities. The whole rock release (Fig. A1a) is a superposition of plagioclase and pyroxene release patterns. We additionally separated and measured vein glass. The release of Ar isotopes can be interpreted as degassing of varying proportions of glass, plagioclase, and pyroxene. In all separates, peaks of trapped ^{36}Ar occur at 450 °C and 700 °C, similar to Dhofar 300 with atmosphere-like $^{36}\text{Ar}/^{40}\text{Ar}$ ratios (see isochron plots, Figs. A2a–d), presumably from the same type of desert alterations. However, some trapped ^{36}Ar is also released at high temperatures.

Similar to Dhofar 300, three isotope plots of Dhofar 007 samples (Figs. A2a–d) demonstrate the presence of trapped Ar with terrestrial atmospheric composition. Correction of the low temperature extractions for air argon again results in more reasonable age spectra for plagioclase and whole rock samples (Figs. A2e–h). However, the pyroxene and glass separates of Dhofar 007 did not yield useful chronological

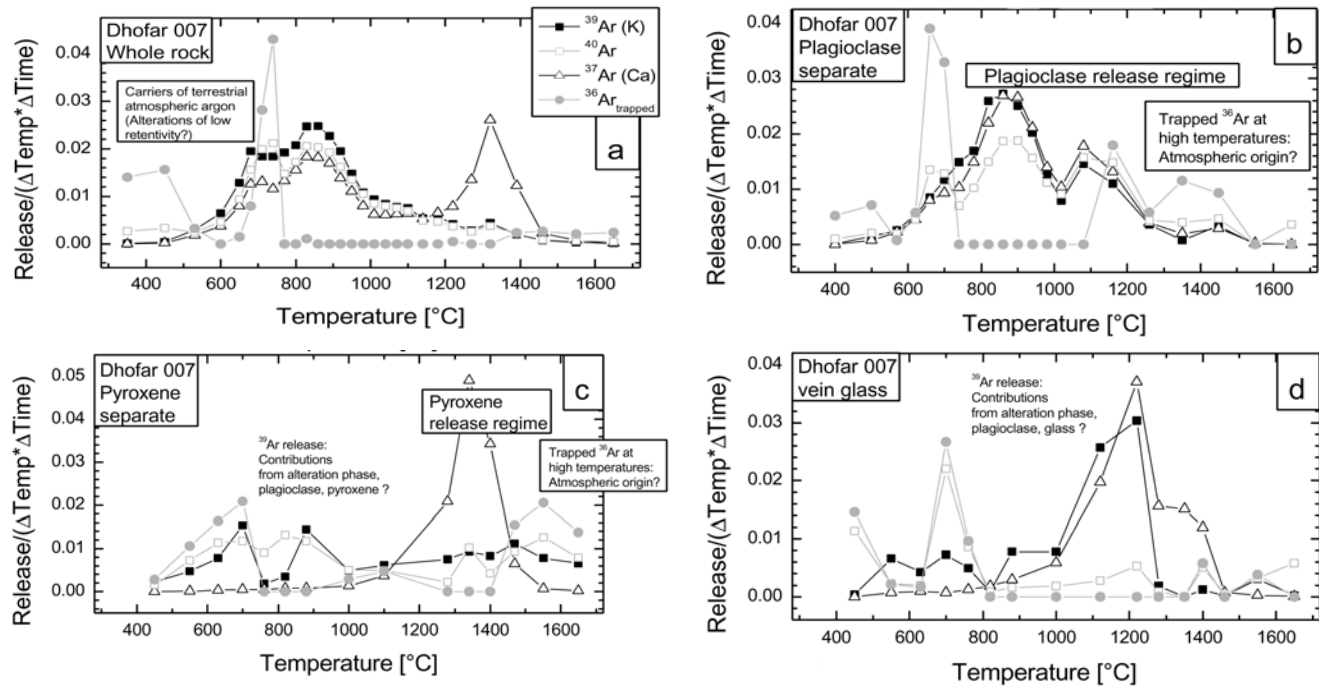


Fig. A1. The release patterns of Ar isotopes for Dhofar 007 samples. Note that in the case of plagioclase and pyroxene separates some trapped ^{36}Ar is released at high temperatures.

data; both low K concentrations and low sample weights (Table 1) cause high uncertainties in the age spectra (Figs. A2g and A2h), so we discuss plagioclase and whole rock age spectra only. Nevertheless, the ^{40}Ar - ^{39}Ar analyses of vein glass has shown that there is no K enrichment in this phase, so we can exclude a significant influence of this minor phase on the whole rock age information.

NWA 011 Ar Carrier Phases

Based on the analyses of the Dhofar 300 and 007 mineral separates and whole rock samples, the fractional argon release of the NWA 011 whole rock sample (Fig. A3) can be interpreted more easily. At high temperatures, there are ortho- and clinopyroxene release peaks dominated by Ca-derived ^{37}Ar . At intermediate temperatures, both Ca-derived ^{37}Ar and K-derived ^{39}Ar degas from plagioclase. However, note that in this temperature range phosphates and silica may also degas. Similar to the Dhofar 300 and Dhofar 007 eucrites, there are peaks at low temperatures of 450 °C and 700 °C containing trapped Ar, but some K and in situ radiogenic argon are also present in the 700 °C peak. The trapped Ar is of atmospheric composition, as revealed by the three isotope correlation diagram (Fig. 8a).

Appendix Tables A1–A5 display measured Ar isotopes corrected for mass discrimination, sensitivity, system blanks, decay, and relative neutron doses. All isotopes are also corrected for interfering isotopes produced on K and Ca during irradiation. Remaining argon isotopes are given in ccmSTP/g and have the following composition:

$$\begin{aligned}
 {}^{36}\text{Ar} &= {}^{36}\text{Ar}_{\text{atm}} + {}^{36}\text{Ar}_{\text{trap}} + {}^{36}\text{Ar}_{\text{cos}} & \text{atm: terrestrial atmospheric Ar} \\
 {}^{37}\text{Ar} &= {}^{37}\text{Ar}_{\text{Ca}} & \text{trap: trapped extraterrestrial Ar} \\
 {}^{38}\text{Ar} &= {}^{38}\text{Ar}_{\text{atm}} + {}^{38}\text{Ar}_{\text{trap}} + {}^{38}\text{Ar}_{\text{cos}} + {}^{38}\text{Ar}_{\text{Cl}} & \text{cos: cosmogenic Ar} \\
 {}^{39}\text{Ar} &= {}^{39}\text{Ar}_{\text{K}} & \text{Ca: Ar derived from Ca} \\
 {}^{40}\text{Ar} &= {}^{40}\text{Ar}_{\text{rad}} + {}^{40}\text{Ar}_{\text{atm}} + {}^{40}\text{Ar}_{\text{trap}} & \text{Cl: Ar derived from Cl} \\
 & & \text{K: Ar derived from K} \\
 & & \text{rad: in situ radiogenic Ar}
 \end{aligned}$$

The apparent ages in tables were calculated by subtracting an almost negligible amount of primordial trapped Ar from ^{40}Ar , assuming that $^{40}\text{Ar}/^{36}\text{Ar} = 1$ in each temperature extraction.

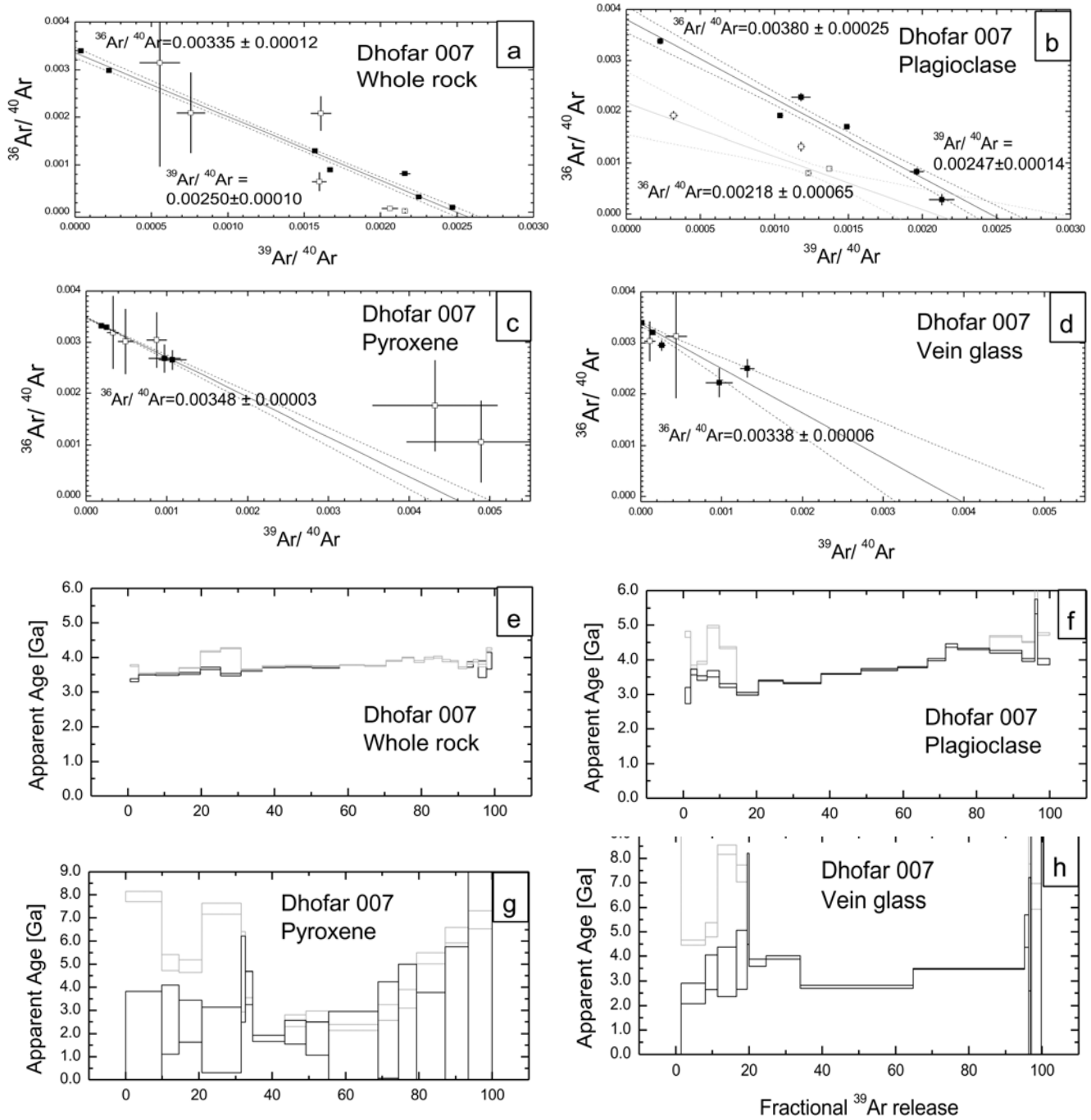


Fig. A2. a-d) Three isotope correlation diagrams $^{36}\text{Ar}/^{40}\text{Ar}$ versus $^{39}\text{Ar}/^{40}\text{Ar}$ ratios for Dhofar 007 demonstrate that trapped ^{40}Ar is of atmospheric composition. Open/closed symbols: high/low temperature extractions. e-h) Age spectra of Dhofar 007 before and after correction for the trapped component identified by the three isotope correlation plots.

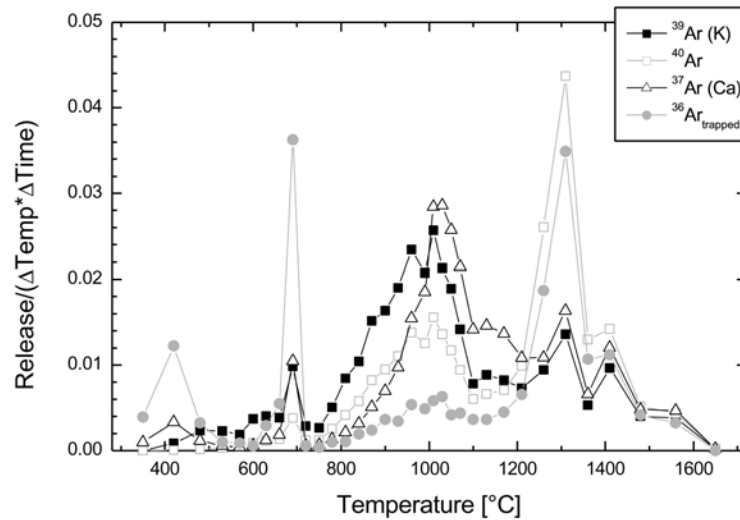


Fig. A3. Degassing pattern of argon isotopes of NWA 011 whole rock sample.

Table A1. Dhofar 007 whole rock.

Temp. (°C)	$^{36}\text{Ar} \times 10^{-12}$	$^{37}\text{Ar} \times 10^{-10}$	$^{38}\text{Ar} \times 10^{-12}$	$^{39}\text{Ar} \times 10^{-12}$	$^{40}\text{Ar} \times 10^{-9}$	Age (Ma)
350	1945 ± 17	0 ± 0	372 ± 5	22 ± 3	569 ± 4	
450	664 ± 6	67 ± 2	189 ± 4	46 ± 3	206 ± 2	7632 ± 114
530	223 ± 4	429 ± 5	205 ± 4	270 ± 5	125 ± 1	3766 ± 26
600	252 ± 4	750 ± 6	379 ± 6	503 ± 5	201 ± 1	3536 ± 9
650	393 ± 7	1152 ± 10	564 ± 6	720 ± 7	292 ± 2	3554 ± 11
680	444 ± 5	1088 ± 9	555 ± 7	656 ± 7	291 ± 2	3698 ± 13
710	691 ± 7	1135 ± 10	614 ± 8	618 ± 7	370 ± 3	4177 ± 15
740	842 ± 8	1001 ± 8	607 ± 6	620 ± 7	394 ± 3	4272 ± 13
770	369 ± 5	1147 ± 9	562 ± 7	646 ± 7	275 ± 2	3631 ± 11
800	434 ± 6	1348 ± 12	657 ± 8	699 ± 8	320 ± 2	3746 ± 13
830	512 ± 7	1587 ± 13	771 ± 8	831 ± 8	384 ± 3	3760 ± 11
860	503 ± 7	1575 ± 13	765 ± 8	834 ± 8	378 ± 3	3732 ± 11
890	461 ± 6	1466 ± 13	726 ± 7	764 ± 8	358 ± 3	3784 ± 11
920	377 ± 6	1199 ± 10	596 ± 6	656 ± 8	301 ± 2	3752 ± 16
950	301 ± 5	960 ± 8	480 ± 5	497 ± 7	252 ± 2	3907 ± 17
980	221 ± 4	691 ± 6	357 ± 5	363 ± 4	195 ± 2	3996 ± 14
1010	187 ± 5	540 ± 6	297 ± 5	315 ± 6	158 ± 1	3885 ± 28
1040	177 ± 5	528 ± 6	285 ± 6	281 ± 5	149 ± 1	3977 ± 25
1070	183 ± 5	546 ± 6	297 ± 5	261 ± 5	141 ± 1	4007 ± 26
1100	185 ± 5	549 ± 7	291 ± 6	254 ± 5	129 ± 1	3908 ± 30
1140	205 ± 6	605 ± 8	329 ± 5	241 ± 4	121 ± 1	3893 ± 22
1180	273 ± 7	755 ± 11	442 ± 7	261 ± 6	116 ± 2	3701 ± 29
1220	355 ± 4	907 ± 8	536 ± 6	189 ± 5	92 ± 1	3842 ± 41
1270	750 ± 9	1945 ± 17	1155 ± 10	157 ± 4	79 ± 1	3906 ± 40
1320	1545 ± 16	3761 ± 32	2341 ± 18	250 ± 6	116 ± 1	3768 ± 38
1390	1104 ± 28	2475 ± 58	1613 ± 38	156 ± 5	98 ± 2	4247 ± 36
1460	263 ± 26	460 ± 42	305 ± 28	57 ± 6	35 ± 3	4229 ± 66
1550	156 ± 44	187 ± 42	142 ± 32	26 ± 7	35 ± 8	5498 ± 209
1650	115 ± 89	33 ± 20	49 ± 31	17 ± 11	30 ± 18	6033 ± 413
Total	14,130 ± 110	28,890 ± 100	16,479 ± 74	11,208 ± 34	6211 ± 22	4050 ± 32

^{40}Ar - ^{39}Ar dating and cosmic ray exposure time of desert meteorites

Table A2. Dhofar 007 plagioclase.

Temp. (°C)	$^{36}\text{Ar} \times 10^{-11}$	$^{37}\text{Ar} \times 10^{-9}$	$^{38}\text{Ar} \times 10^{-11}$	$^{39}\text{Ar} \times 10^{-12}$	$^{40}\text{Ar} \times 10^{-9}$	Age (Ma)
400	272 ± 5	2 ± 1	56 ± 3	183 ± 17	791 ± 10	7582 ± 163
500	109 ± 3	50 ± 1	45 ± 2	471 ± 27	397 ± 6	4741 ± 91
570	36 ± 2	96 ± 3	45 ± 2	558 ± 25	262 ± 5	3785 ± 63
620	79 ± 3	138 ± 2	73 ± 2	862 ± 24	439 ± 6	3914 ± 39
660	261 ± 4	197 ± 3	131 ± 4	1081 ± 24	1040 ± 13	4962 ± 31
700	234 ± 4	228 ± 3	132 ± 2	1484 ± 27	991 ± 12	4354 ± 23
740	78 ± 3	252 ± 4	119 ± 2	1893 ± 39	543 ± 7	3031 ± 22
780	107 ± 3	365 ± 5	174 ± 3	2158 ± 38	791 ± 10	3401 ± 18
820	168 ± 4	538 ± 7	262 ± 5	3301 ± 47	1153 ± 14	3326 ± 12
860	200 ± 4	661 ± 8	315 ± 5	3464 ± 53	1439 ± 17	3593 ± 16
900	196 ± 4	651 ± 9	297 ± 5	3197 ± 47	1446 ± 17	3726 ± 14
940	149 ± 5	517 ± 7	254 ± 5	2574 ± 42	1208 ± 14	3785 ± 18
980	96 ± 2	342 ± 5	165 ± 4	1608 ± 36	866 ± 11	4004 ± 30
1020	71 ± 3	255 ± 4	123 ± 3	1008 ± 33	698 ± 9	4414 ± 49
1080	200 ± 4	652 ± 7	312 ± 4	2782 ± 46	1816 ± 17	4317 ± 22
1160	380 ± 6	642 ± 7	336 ± 5	2811 ± 50	2286 ± 21	4681 ± 25
1260	155 ± 3	241 ± 3	137 ± 2	1151 ± 19	836 ± 11	4494 ± 16
1350	170 ± 6	113 ± 3	83 ± 3	220 ± 20	689 ± 15	7011 ± 153
1450	178 ± 9	179 ± 5	113 ± 4	1067 ± 35	906 ± 23	4753 ± 36
1550	233 ± 29	15 ± 2	51 ± 6	0 ± 0	763 ± 66	
1650	246 ± 87	0 ± 0	61 ± 19	6 ± 6	690 ± 180	
Total	3618 ± 94	6133 ± 22	3285 ± 25	31,880 ± 160	20,060 ± 200	4193 ± 559

Table A3. Dhofar 300 whole rock.

Temp. (°C)	$^{36}\text{Ar} \times 10^{-12}$	$^{37}\text{Ar} \times 10^{-10}$	$^{38}\text{Ar} \times 10^{-12}$	$^{39}\text{Ar} \times 10^{-12}$	$^{40}\text{Ar} \times 10^{-9}$	Age (Ma)
300	970 ± 10	13 ± 1	196 ± 2	31 ± 1	302 ± 2	9015 ± 83
450	1337 ± 9	31 ± 1	302 ± 3	297 ± 3	395 ± 2	5516 ± 15
530	424 ± 6	91 ± 1	194 ± 2	823 ± 8	127 ± 1	2185 ± 8
600	336 ± 4	190 ± 3	238 ± 3	706 ± 6	116 ± 1	2257 ± 5
650	284 ± 4	249 ± 3	219 ± 3	545 ± 5	122 ± 1	2673 ± 9
680	307 ± 6	211 ± 4	193 ± 4	358 ± 7	119 ± 2	3248 ± 9
710	555 ± 10	415 ± 7	386 ± 7	592 ± 10	215 ± 4	3383 ± 6
740	694 ± 12	631 ± 11	581 ± 10	720 ± 12	291 ± 5	3549 ± 7
770	331 ± 6	528 ± 9	459 ± 8	593 ± 11	182 ± 3	3130 ± 10
800	455 ± 8	740 ± 12	662 ± 11	778 ± 13	250 ± 4	3202 ± 4
830	544 ± 9	891 ± 15	793 ± 13	972 ± 16	342 ± 5	3336 ± 5
860	687 ± 12	1117 ± 18	1003 ± 17	1274 ± 21	469 ± 7	3406 ± 6
890	735 ± 13	1216 ± 20	1098 ± 18	1440 ± 25	545 ± 9	3448 ± 9
920	744 ± 13	1227 ± 20	1117 ± 19	1495 ± 24	586 ± 9	3503 ± 5
950	917 ± 16	1531 ± 25	1375 ± 22	1923 ± 31	758 ± 12	3511 ± 6
980	770 ± 13	1274 ± 21	1177 ± 20	1718 ± 28	671 ± 11	3497 ± 4
1010	777 ± 14	1281 ± 22	1180 ± 20	1720 ± 28	692 ± 11	3542 ± 6
1040	714 ± 13	1133 ± 19	1055 ± 18	1508 ± 25	610 ± 10	3553 ± 6
1070	768 ± 14	1179 ± 20	1134 ± 19	1478 ± 25	620 ± 10	3609 ± 6
1100	897 ± 18	1221 ± 24	1258 ± 24	1429 ± 27	621 ± 12	3664 ± 5
1130	1644 ± 29	2072 ± 35	2432 ± 41	1642 ± 27	701 ± 11	3635 ± 6
1160	2752 ± 48	3726 ± 63	4158 ± 69	2185 ± 36	965 ± 16	3688 ± 6
1190	3381 ± 59	4983 ± 84	5100 ± 84	2921 ± 48	1373 ± 22	3787 ± 5
1220	1842 ± 33	2766 ± 47	2807 ± 47	2080 ± 35	975 ± 16	3783 ± 7
1250	1665 ± 29	2547 ± 43	2511 ± 42	2209 ± 37	1074 ± 17	3840 ± 8
1280	342 ± 7	550 ± 10	538 ± 10	559 ± 10	263 ± 4	3788 ± 9
1310	1213 ± 22	1929 ± 33	1826 ± 31	2040 ± 34	1012 ± 16	3872 ± 5
1360	302 ± 6	504 ± 9	466 ± 8	517 ± 9	261 ± 4	3900 ± 10
1420	416 ± 7	701 ± 10	641 ± 9	666 ± 9	332 ± 4	3881 ± 6
1480	5 ± 4	19 ± 6	14 ± 4	4 ± 2	5 ± 1	5137 ± 504
1550	22 ± 5	1 ± 1	0 ± 0	1 ± 1	9 ± 1	8485 ± 1087
Total	26,830 ± 110	34,970 ± 150	35,110 ± 150	35,230 ± 120	15,001 ± 52	3632 ± 2

Table A4. Dhofar 300 pyroxene.

Temp. (°C)	$^{36}\text{Ar} \times 10^{-11}$	$^{37}\text{Ar} \times 10^{-10}$	$^{38}\text{Ar} \times 10^{-11}$	$^{39}\text{Ar} \times 10^{-12}$	$^{40}\text{Ar} \times 10^{-9}$	Age (Ma)
450	881 ± 14	58 ± 7	177 ± 3	278 ± 11	2593 ± 38	8957 ± 68
550	65 ± 1	52 ± 4	20 ± 1	244 ± 8	204 ± 4	4720 ± 50
630	142 ± 2	120 ± 7	36 ± 1	301 ± 8	434 ± 7	5656 ± 38
700	330 ± 5	182 ± 6	78 ± 2	546 ± 12	998 ± 15	6064 ± 28
760	34 ± 1	201 ± 9	22 ± 1	362 ± 15	133 ± 5	3404 ± 33
820	29 ± 1	280 ± 11	29 ± 1	368 ± 16	142 ± 5	3481 ± 37
880	31 ± 1	379 ± 15	36 ± 1	489 ± 19	181 ± 6	3416 ± 31
940	27 ± 1	363 ± 14	36 ± 1	388 ± 15	181 ± 6	3777 ± 31
1000	31 ± 1	387 ± 15	38 ± 1	458 ± 17	185 ± 6	3547 ± 22
1060	43 ± 2	517 ± 19	55 ± 2	550 ± 20	212 ± 7	3480 ± 19
1120	79 ± 3	921 ± 33	106 ± 4	543 ± 21	211 ± 7	3491 ± 32
1160	166 ± 6	1865 ± 64	242 ± 8	412 ± 16	182 ± 6	3687 ± 33
1200	365 ± 12	4960 ± 170	546 ± 18	494 ± 19	235 ± 8	3806 ± 32
1240	301 ± 11	4120 ± 140	448 ± 16	319 ± 14	154 ± 5	3832 ± 47
1280	148 ± 6	1961 ± 79	217 ± 9	132 ± 11	79 ± 3	4185 ± 123
1320	188 ± 8	2730 ± 110	286 ± 12	155 ± 10	77 ± 3	3876 ± 82
1380	140 ± 4	2016 ± 58	211 ± 6	219 ± 10	85 ± 2	3484 ± 59
1450	31 ± 2	437 ± 33	44 ± 3	24 ± 7	24 ± 2	4998 ± 503
Total	3033 ± 26	21,560 ± 280	2630 ± 31	6283 ± 62	6311 ± 46	5035 ± 38

Table A5. Dhofar 300 plagioclase.

Temp. (°C)	$^{36}\text{Ar} \times 10^{-11}$	$^{37}\text{Ar} \times 10^{-10}$	$^{38}\text{Ar} \times 10^{-11}$	$^{39}\text{Ar} \times 10^{-11}$	$^{40}\text{Ar} \times 10^{-9}$	Age (Ma)
400	625 ± 15	42 ± 7	123 ± 3	13 ± 1	1847 ± 43	9680 ± 123
500	243 ± 6	213 ± 7	64 ± 2	50 ± 2	746 ± 18	5721 ± 45
560	108 ± 3	217 ± 10	37 ± 1	30 ± 1	374 ± 9	5395 ± 50
610	173 ± 4	413 ± 14	61 ± 2	58 ± 2	578 ± 14	5035 ± 37
650	246 ± 6	414 ± 14	78 ± 2	51 ± 2	801 ± 19	5793 ± 37
680	191 ± 5	452 ± 13	69 ± 2	57 ± 2	639 ± 15	5237 ± 32
710	188 ± 5	607 ± 16	81 ± 2	76 ± 2	656 ± 16	4788 ± 24
740	87 ± 3	624 ± 18	68 ± 2	71 ± 2	384 ± 9	4011 ± 27
770	103 ± 3	1023 ± 28	102 ± 3	128 ± 3	536 ± 13	3608 ± 11
800	96 ± 3	1167 ± 32	115 ± 3	148 ± 4	573 ± 14	3486 ± 10
830	123 ± 3	1747 ± 44	162 ± 4	204 ± 5	809 ± 19	3524 ± 12
860	158 ± 4	2373 ± 59	219 ± 5	279 ± 7	1106 ± 26	3520 ± 10
890	170 ± 3	2585 ± 37	237 ± 3	309 ± 4	1229 ± 15	3526 ± 9
920	169 ± 3	2587 ± 35	239 ± 3	313 ± 4	1269 ± 15	3556 ± 9
950	158 ± 3	2483 ± 35	226 ± 3	305 ± 4	1243 ± 15	3563 ± 10
980	164 ± 3	2615 ± 39	237 ± 4	320 ± 4	1336 ± 16	3603 ± 9
1010	136 ± 2	2083 ± 33	191 ± 3	243 ± 4	1087 ± 13	3707 ± 13
1040	127 ± 2	2016 ± 28	183 ± 3	251 ± 3	1088 ± 13	3661 ± 8
1070	161 ± 3	2530 ± 38	232 ± 3	325 ± 4	1447 ± 17	3702 ± 7
1100	119 ± 2	1925 ± 28	176 ± 3	264 ± 4	1199 ± 14	3733 ± 10
1130	119 ± 2	1885 ± 29	174 ± 3	271 ± 4	1263 ± 15	3773 ± 11
1160	126 ± 2	1941 ± 30	182 ± 3	282 ± 4	1361 ± 16	3829 ± 9
1190	165 ± 3	2649 ± 39	240 ± 3	371 ± 5	1826 ± 21	3861 ± 8
1220	164 ± 3	2703 ± 38	243 ± 3	378 ± 5	1890 ± 22	3885 ± 10
1250	158 ± 3	2645 ± 39	240 ± 3	386 ± 5	1908 ± 23	3868 ± 6
1280	140 ± 3	2386 ± 35	215 ± 3	316 ± 5	1574 ± 19	3880 ± 13
1310	123 ± 1	2074 ± 16	189 ± 1	278 ± 2	1417 ± 3	3918 ± 8
1360	176 ± 2	2981 ± 20	268 ± 2	371 ± 2	1940 ± 3	3957 ± 7
1450	1001 ± 5	16,785 ± 58	1514 ± 6	2071 ± 6	10,557 ± 10	3916 ± 4
1550	16 ± 3	169 ± 10	20 ± 1	31 ± 2	186 ± 7	4180 ± 71
Total	5734 ± 23	64,330 ± 170	6184 ± 17	8247 ± 20	42,869 ± 95	3947 ± 7